FINAL REPORT

Contract NAG 5-161
National Aeronautics and Space Administration

COMPARISON OF ENVIRONMENTAL CONDITIONS IN THE BERING SEA AND DAVIS STRAIT AND THE EFFECTS ON MICROWAVE SIGNATURE RETURNS; MARCH AND APRIL, 1979

by
S. Lyn McNutt
Department of Geography
University of Washington
Seattle, Washington 98195

15 June 1982

Principal Investigator: Seelye Martin
School of Oceanography
University of Washington
Seattle, Washington 98195

Ref: A82-13

Table of Contents

Abstract

Aircraft data collected in the Bering Sea in March, 1979 using a 6.6 GH_z (C Band) microwave radiometer and a 13.9 GH_z (Ku Band) scatterometer, reinforce the difficulties in interpreting first year ice types found near the ice edge in a marginal ice zone. An ice interpretation scheme using data taken with a 13.3 GH_z (Ku Band) scatterometer and a 19.4 GH_z (K Band) radiometer in Davis Strait also shows ambiguity in the first year ice signal and indicates that ice interpretation becomes more difficult near the ice edge and under warmer conditions. This report also compares X Band SAR data taken in Davis Strait with similar imagery collected in the Bering Sea. Ice core samples from the Bering test area offer a basis for speculation on changes in ice morphology which affect the signature return at the ice edge, and help explain the difficulty of the sensors in discerning the two different ice types found on the photography and in the core samples.

1.0 Introduction

Recent ice investigations reflect an interest in the marginal ice zone (MIZ), areas where there is a seasonal ice edge whose position and characteristics vary considerably over time. The Bering Sea and Davis Strait are two such regions located in the western and eastern Arctic respectively. Being qualitatively similar, they allow researchers to compare ice types and processes to see if similarities exist from one geographic location to another, and they offer opportunities to study processes in areas composed of ice which is typically thin compared to arctic pack ice.

Most sea ice research has been directed at understanding properties in the central Arctic pack. Livingstone et al (1981) devised an ice signature identification scheme which delimits eleven World Meteorology Organization (WMO, 1970) ice classes. This method is temperature dependent and works best in the central arctic with consistently low temperatures and large fields of similar ice types. Hawkins et al (1980) state that the results break down at temperatures greater than -2°C. Limited data analysis conducted in Davis Strait adds information from first-year ice, taken at the ice edge, to this scheme, but indicates that ambiguities exist in interpreting these results using the first-year ice signatures obtained in the Beaufort Sea. A data set taken in the Bering Sea under similar conditions augments the information obtained in previous studies, but fails to resolve the problems associated with defining a distinctive signature for first-year ice found near the edge under melting conditions.

This report discusses the analysis done on the Bering Sea data set and compares it to the existing results. The availability of better groundtruth, in the form of ice core samples, allows for speculation concerning the ice identification problems. Specifically, section 2.0 compares the environmental

climatology of the regions and some morphological differences in the surface features of the ice found there. Section 3.0 discusses the two experiments involved, their instrumentation, and the problems encountered in the data collection. The comparisons of data results found in section 4.0 include a discussion of the Bering Sea ice core samples and speculations on the ice properties affecting the return. Concluding remarks are in section 5.0.

2.0 Environmental Climatology

Both the Bering Sea and Davis Strait exhibit similar characteristics as marginal ice zones. Differences do exist, the most notable being the more northerly latitude of the Davis Strait ice zone which begins at ~66°N and extends to the North Water area at ~76°N. The Bering Sea ice cover reaches ~58°N, and, for purposes of this study, terminates at the Bering Strait ~66°N. In the Bering Sea, all ice formed is first year ice which melts back completely each season. Davis Strait contains some icebergs as well as second year and multiyear ice, but first-year ice comprises the majority of the pack. The first-year ice melts back most seasons except for remnant fast ice in the colder years. Differences like these, including other related environmental conditions, affect ice morphology, and may alter the signal return of remote sensors.

2.1 The Bering Sea

The Bering Sea divides into water overlying an abyssal plain for one-half its extent, the other half being an extensive shelf area, the Bering basin, including Norton Sound in the northeast (Kinder, 1980) (figure 1). This study confines itself to the shelf area and emphasizes processes in the eastern half of the sea.

The water generally circulates northward, but the transport speeds vary over the area and change with time (Coachman et al, 1975). The currents move fastest in the straits (Anadyr, Bering, and between the eastern portion of St. Lawrence Island and the Alaska mainland) where the water converges, and accelerates around projecting land masses. Southerly water flow through Bering Strait does occur especially in fall and early winter (Coachman and Aagaard, 1980). In heavy years, the ice extends nearly to the shelf break at the 150 m contour. Its maximum advance depends in part on the location of the Bering slope current which parallels the shelf break (Kinder et al, 1975; Schumacher et al, 1979). At the beginning of freeze up in Norton Sound, Muench et al (1980) report that the water consists of two layers separated by a strong pyncnocline, the upper layer being warmer and less saline. By mid-winter, the Bering basin is vertically homogeneous in salinity and temperature (Newton and Andersen, 1980).

A continental, arctic climate characterizes the winter months, replaced by maritime influences in the summer (Overland, 1980). In heavy ice years, fewer storms occur north of 60°N latitude and cold air from Alaska and the Arctic produces dominant winds from the N-NE. Generally, more storms occur in light ice years, propagating up the Siberian side bringing more winds from the S-SW (Overland and Pease, 1981) (figure 2).

Fast ice forms in October in quiescent areas such as Norton Bay, and advances during November-December. This ice generally extends to the 20 m contour, coincident with a grounded ridge at its terminus (Stringer, 1980) (figure 3). Maximum extent of the pack ice occurs in mid-February to March changing to spring decay in April-June (Dunbar, 1967). In December-February the ice advances to the S-SW under N-NE wind conditions forming polynyas on the leeward side of east-west trending coasts. Polynyas recur seasonally to

the south of the coast near Nome, south of St. Lawrence Island, and south of Nunivak and St. Matthew Islands as the ice reaches maximum extent.

The grease ice generated in these polynyas thickens downwind, congeals to form floes and migrates southward at approximately 28-40° to the right of the wind direction (Loschilov, 1974; Campbell et al, 1974, Muench and Ahlnäs, 1976; McNutt, 1980, 1981). Although these conditions predominate during February to March, occasional storms from the S-SW close the pack ice, fill the polynyas and push the floes northward. At the ice edge, the ice cover interacts with the incoming swell, breaking into smaller floes and forming ice bands which migrate downwind faster than the interior pack ice (Martin et al, 1983). As this ice encounters warmer water, it melts, and the location of this warmer water determines the ice edge limit throughout the season (Pease, 1980). During ice advance, the pack may turn over from two to five times (Pease, 1980).

The character of the ice edge is important in understanding the ice signature of ice found in this area. The ocean swell fractures ice advected from the interior pack. This ice consists of thick and thin white ice as well as gray-white and grey ice formed in between the advancing thicker ice as it spreads out downwind in the wider, southern end of the basin. At the edge, the ice breaks into small rough floes which measure 10-20 m across and raft to 1-5 m thick (Bauer and Martin, 1980; Squire and Moore, 1981; Martin et al, 1983). These floes move to open water under off-ice winds forming bands typically 1-10 km in length and 0.1 to 1 km wide (Muench and Charnell, 1977). These orient at approximately right angles to the wind. Generally, ice at the edge consists of three zones (Bauer and Martin, 1980): the edge zone, 5-10 km wide consisting of small, broken floes; the transition zone, ~5 km wide with small, rectangular floes; and the interior zone ~100 km in extent

with large floes (figure 4). The widths of the zones vary depending on the intensity of the incoming swell and its ability to fracture the ice. These conditions were present in the March, 1979 study. Off-ice winds produce a diffuse edge with many ice bands which move downwind and ablate; on-ice winds compact the floes at the edge, but generally bring increased swell activity fracturing the ice further into the pack while pushing floes against each other. Generally, melt and decay of the ice characterizes the region at the edge, but the onset of cold conditions causes refreezing of the surface layers of the water and the ice.

Ice retreat begins when warmer air arrives from the south and combines with the seasonal increase in solar insolation. The edge migrates northward, ice production stops in the southerly polynyas and they close as new polynyas open to the north, or leeward side, of the coasts, especially St. Lawrence Island and southern and eastern Norton Sound. The ice generally moves northward, however, in April-May, 1980 the author observed a reversal of this flow on satellite pictures where a massive influx of thick ice from the Chukchi Sea broke through Bering Strait and advanced southward, rapidly reoccupying previously ice-free areas.

2.2 Davis Strait

Davis Strait overlies an area of deep water and receives ice from many sources including Lancaster Sound, Jones Sound, Smith Sound and Baffin Bay (figure 5). The coastlines of the areas bounding the Strait have high relief and often contain fjords and glacial snouts which calve into ice source regions. This means the ice cover often contains second year ice, multiyear ice and icebergs, bergy bits and growlers. The increased relief compounds the local wind field introducing katabatic wind effects.

The ocean current regime differs significantly from the Bering Sea (figure 6). Dunbar (1972) proposes three different types of current regimes which affect ice edge locations in the Northern Hemisphere: warm, northward-flowing currents flowing toward the ice (Norwegian and Barents Seas); cold, southward currents moving away from the ice and advecting ice with them (Greenland Sea); and currents which flow along the ice edge, parallel to it (Bering Sea). All three types interact in Davis Strait. In the east, heat transport from the northward flowing West Greenland current limits the ice advance. The cold Labrador current carries western ice southward to the eastern coast of Newfoundland. A current parallel to the ice edge limits the middle portion of the ice, but unlike the Bering Sea, it acts as a southwestward moving stream which deflects ice into the Labrador current. Because of this system, the total width of the ice extent does not vary much with changes in current. As the warm Greenland current increases, the Labrador flow increases, carrying more ice southward into warmer waters. In this case, warmer water causes greater ice production due to advection, but the ice melts faster creating a self-regulating system. This may account for the consistency in the yearly ice edge location in Davis Strait (Dunbar, 1972; Eastern-Western Arctic Sea Ice Analyses, 1977, 1978, 1979). In contrast, the ice edge location in the Bering Sea varies considerably when the ice reaches its yearly maximum (Webster, 1981).

Maxwell (1981) describes this area as the only climatological sub-region in the Canadian Arctic which is marine. The mean cyclone trajectory governing weather for this area passes over the eastern half of Davis Strait (figure 7). Frequent storms occur over all seasons often injecting milder air, and the high relief of the surrounding area produces strong local variations in wind and temperature. These frequent storms and changes in temperature during the

season confuse any easy definition of ice morphology in the area, making ice thickness distritutions and surface roughness characteristics more complex than the apparent system in the Bering Sea. The additional storms also bring heavier snowfall.

Crane (1978) discusses the synoptic climatology of the area and describes two different ice scenarios during freeze-up and decay which may cause different ice morphologies to dominate during those times. An early ice advance brings a large influx of second-year and multiyear ice from Baffin Bay. Ice in Davis Strait arrives from the north and includes ice which travels east along Hudson Strait to Foxe Basin. Winds from the east, north and west predominate. New ice growth in Frobisher Bay and Ungava Bay characterizes ice during a late advance. Ocean swell breaks up this ice and rafts it as the ice extends seaward. Thin, new ice dominates through the early part of the season. There are more of the warmer easterly winds during this situation and less northerly or westerly flow. In both cases, the water along the Labrador coast is the last to freeze (figure 8). In an early ice retreat, the ice begins to melt back during mid to late August. Southerly winds dominate. A late retreat leaves remnant ice in Frobisher Bay and near Cumberland Pennisula in September. Less storms with southerly airflow penetrate during this scenario. Also, ice involved in a late retreat shows more variation in its advance. No correlation exists which prescribes that an early freeze-up necessitates a late retreat or vice versa.

The general ice freeze-up and retreat pattern is similar to the Bering Sea with some important differences. Freeze-up begins with the fast ice areas located in protected bays and fjords in mid to late October, earlier than the Bering. The water, having a salinity similar to the Bering Sea, approximately 32°/oo, requires a similar temperature to begin freezing, ~-1.8°C (Collin and

Dunbar, 1964). Ice formation begins in the north and progresses southward. The fast-ice contour occurs at 180 m off the east coast of Baffin Island (Jacobs et al, 1975) (figure 9), but water currents continually move ice off Cape Dyer, and no general rule exists for fast ice limits as in the Bering. Another significant difference lies in the amount of second year and multiyear ice contained in the fast ice. There is none in Bering Sea fast ice, but in Davis Strait an increasing proportion of older ice occurs in more northern areas.

Maximum ice extent occurs in March to April, later than the Bering Sea (Dunbar, 1972). After the initial freeze-up, the ice advances off the coasts from the west to east and moves from north to south partly from ice formed in the recurrent North Water polynya (Dunbar, 1973; Crawford and Parkinson, 1980). Dey (1981) indicates considerable ice transport into Davis Strait from ice originating in Smith Sound. Ito and Müller (1982), tracing floe motions for ice at maximum extent, show that a general southward movement of ice exists under northerly wind conditions. The position of the ice edge at maximum extent does not vary considerably from year to year, but the ice advected southward changes in extent and varies in thickness and morphology throughout the season.

Changes in incoming solar radiation, tides, and the onset of storm activity bring on the ice breakup (Jacobs et al, 1975). The meltback proceeds from south to north and north to south simultaneously as the ice edge retreats and the North Water polynya opens up. Home Bay has ice the longest, often into August (Maxwell, 1981), but the area is generally ice-free by late August to early September, much later than the Bering Sea.

3.0 Description of the Two Experiments and Instrumentation

Two different groups of researchers, NASA and CCRS, conducted experiments under similar conditions in 1979 in the Bering Sea and Davis Strait. Both flew aircraft equipped with remote sensing instruments over the ice at the edge. In the Bering, a ship stationed at the edge equipped with a helicopter allowed scientists to gather detailed core reports on ice conditions during the entire cruise 2 to 14 March. Difficulty landing a surface truth party using a shore-based helicopter limited the Davis Strait ice core measurements to two samples. Significant differences existed in the two flight patterns used to collect data, with the Davis Strait pattern being more useful for judging ice conditions.

3.1 Bering Sea Experiment

The Bering Sea flight occurred on 14 March 1979. Groundtruth data collection took place from the NOAA ship SURVEYOR stationed at the ice edge from 2 to 14 March. Personnel entered the ice field using boats and a helicopter launched from the ship. Salo et al (1980) present a complete analysis of the ship's data. Researchers from Scott Polar Research Institute collected data on the response of the floes to incoming swell (Wadhams and Squire, 1980). The NASA C130 aircraft flew over the area and collected data using a 13.9 GH_z (Ku Band) scatterometer (Jones et al, 1977), a 6.6 GH_z (C Band) radiometer (Harrington, 1979) and an RC 9 camera. Later in the day, the NASA C131 flew over the same area with an X Band SAR (Schertler, 1978). Figure 10 shows the flightline for the C130; the flightline for the C131 appears in figure 40.

In retrospect, the shape of the flightline chosen combined with the diffuse nature of the ice edge made data analysis difficult. Problems also

arose in the time codes on the sensors so that five minute data runs reduced to a maximum of three minutes of usable data. Comparison of the radiometer and scatterometer data to the airphotos left many gaps as each track contained considerable open water. Also, the low-altitude flights for laser runs precluded airphoto analysis because the photographs did not overlap. Further, in an attempt to simulate the 6 angle simultaneous data collection mode of the CCRS scatterometer, NASA operators changed the look angle on the scatterometer every five seconds on some runs. Under such diffuse ice conditions, one ice type rarely filled the sampling footprint, and angular dependence studies were not statistically valid. The data reduced to one run where the scatterometer angle remained at 58° and photographic overlap existed. The radiometer data applied to all runs where photos existed, and provide more valid statistics.

3.2 Davis Strait Experiment

This program also studied the physical properties of the sea ice, floe flexure and heave response and meteorological parameters (Gray et al., 1979). On 10 April, 1979 the Canadian Centre for Remote Sensing (CCRS) flew a 19.4 GH_z (K Band) radiometer and a 13.3 GH_z (Ku Band) scatterometer over the ice while collecting simultaneous airphotos. The Naval Oceanography Research and Development Activity (NORDA) P3 covered the same area with an X Band radar (Ketchum and Farmer, 1980).

The flightline (figure 11) differed from the Bering Sea line by heading straight into the pack from the open water side. This allows data to be collected at the edge under melting conditions and further into the pack providing a signature on the non-melting ice. The ice at the edge was more deteriorated than the Bering ice, and groundtruth includes only two ice cores (Gray et al, 1979; Wadhams and Squire, 1980). The cores imply that the ice

differs from the Bering Sea since it had more snow accumulated at the surface. Photos obtained from the CCRS aircraft also show compact ice at the edge with little ice band formation preceding the overflight.

4.0 Comparison of Data Results and Ice Conditions

The Bering Sea ice edge consisted of ice bands moving downwind under conditions which persisted for several days prior to the overflight. This resulted in a well-developed diffuse ice edge with two types of ice present: rafted white ice floes which appeared dry and large grey-white floes with wet surfaces. In contrast, the Davis Strait edge appeared to be compact with little band formation. The smallest floes occurred at the ice edge, and floe size increased into the pack. For both the ice conditions this section discusses the temperature dependence of the ice interpretation scheme devised by Livingstone et al (1981) and shows that significant surface moisture effects existed at lower temperatures in the Bering Sea. Because of this surface moisture, the emissivity and backscatter failed to resolve the two ice types seen in the photographs and in the ice cores.

4.1 Bering Sea Ice Conditions

Figure 12 taken 13 March 1979 shows the large scale ice generation mechanisms for the Bering Sea described in section 2.1. It is a strip mosaic of LANDSAT images which begins north of St. Lawrence Island and extends past St. Matthew Island to the ice edge. The north shore of St. Lawrence Island has a fast ice edge (marked 1 on the image), a thicker wedge of first year ice extends northward (2) from the fast ice boundary, a polynya (3) on the southern coast generates frazil ice which forms pancakes which then consolidate and the ice thickens downwind where leads begin to open in the

pack (4). The effects of wind and incoming swell combine to create ice bands near the edge (5). McNutt (1980,1981) and Pease (1980) discuss these processes in greater detail.

As seen in figure 4, the ice edge on 14 March consisted of an area of broken floes, a transition zone, and an area of large sheets of pack ice. The aircraft data collected appear to be from these ice band areas as no airphotos show the larger fields of ice. Figure 13 shows an ice band in more detail. The ice adjacent to the water visible in the mosaic is the leading edge of a large ice band. Striations of the floes within the feature show two types of ice present: thicker, small white floes 20-50 m across and larger floes of thinner grey and grey-white ice approximately 200-500 m with some larger. The surface of the grey and grey-white ice can appear white or dark grey depending on the degree of melting of the snow cover. Figure 14 shows the leading edge of another ice band where a sharp distinction between the ice and water exists, and the trailing edge which consists of small floes behind the main body of the band. Martin et al (1983) describe the physical process which causes this difference.

The two ice types mentioned previously show up well in figure 15. The area (1) indicates large grey-white floes still covered with some surface snow while (2) shows grey-white ice with a melted surface. The matrix ice consists of small white floes (3). At a lower altitude, figure 16 shows how much open water and nilas exist between the floes. Snow covers the large white floe in the upper right portion of the mosaic. The surface of the floes appears mottled and contains thaw holes. Figure 17 shows more variations of the surface texture present in the moist surface of the grey-white floes. More detailed surface relief can be seen in figures 18 and 19 taken from the helicopter which had landed on similar ice. The upper layer contains

consolidated pancake ice with some snow drifts. Figure 20 shows that the white floes appear strikingly different. The surface contains ridges with snow drifts and flat, snow covered areas. The snow looks dry compared to the grey-white floes. Martin and Kauffman (1979) report these ridges as 1 m or less and show a surface view in figure 21.

Kauffman and Squire, and Bauer conducted ice surveys with the helicopter on board the NOAA ship SURVEYOR for 13 and 14 March respectively. On the 13th Kauffman and Squire took ice cores and gave a detailed description of the ice conditions encountered. Appendix A reproduces both ice reports and contains a record of the ice floe measurements. The first ice encountered consisted of pieces of thick ice 10-20 m in diameter at 75% concentration. This changed to large floes of new ice 30-50 m at 80%. After crossing an area of open water containing <1% of 10 m diameter floes, another field of 10-30 m floes at 80% concentration appeared. These were thick and snow covered. Large, thin grey ice floes adjoined these with a concentration of 90% with an occasional thick ice floe matrix of about 25%. The record includes one core from each ice type, and Appendix A presents the details of the analysis.

On 14 March, Bauer constructed a diagram of ice conditions encountered preceding the NASA flight. Figure 21 recreates her analysis. She indicates the two types of ice present and adds that the floe size increased away from the edge, noting that some of the open water had grease ice streaks. Grease ice streaks do not appear in the C130 photographs, but the two ice types dominate the imagery. Salo et al (1980) reported the following weather conditions at the time of the overflight: air temperature -5.5°, windspeed 8 ms^{-1} from 55°, water temperature -1.2°C. Similar conditions existed several days previous to the overflight so that the diffuse ice edge/band melt conditions were well-developed.

The ice samples listed as N1 and N2 in Appendix A correspond to the grey-white ice and the white ice respectively. The salinity and temperatures are surface measurements taken for the frazil layer. Figure 23 shows conditions at site N1. The ice surface is wet and slushy. Areas appearing white on other grey-white floes actually consisted of very wet snow. The snow salinity remains low, but the slush layer immediately beneath it retains more salt than the ice surface scrape, which is also quite saline. The ice core (figure 26) shows the 130 mm frazil layer overlying the columnar ice. The brine inclusions and the crystal sizes in the upper layers are quite large ranging from $\leq$ 2 mm to 6 mm in size. The salinity profile with depth shows a definite new, first-year ice character (figure A-1); the temperature vs depth profile indicates that the ice was very warm ranging from -2.1°C at the surface to -1.7°C at the bottom of the floe (Table A-I).

The next set of figures (25 and 26) shows conditions for the core N2, the white ice. The ice surface is dry, with no slush, and contains 330 mm of frazil on top, over one-half the core length (figure A-2). Both the snow and the ice surface have low salinities as does the ice itself, and the temperature profile shows the ice is warm. Weeks and Ackley (1982) describe how brine in first-year ice drains out as the ice warms rapidly, which appears to be the case here. Figure 27 shows the ice core for N1. Since there is no way to tell if all the rafted white ice encountered meets these specifications, table A-1 includes data on ice core B5 taken on 7 March when similar ice conditions existed. Figure 28 shows the 20 m white ice floe for core B5 which can be identified on the floe. Figure 29 shows the surface of the floe and the texture of the surrounding ice. The core sample is similar to N2 but does not contain a second frazil layer beneath the columnar ice. The upper frazil layer is 300 mm deep, well over half the core length (figure A-3). Both floes

have large brine inclusions and crystal sizes in the upper layers, and show evidence of brine drainage. Core B5 is both more saline and colder (figure 30). The snow layer and ice surface have a higher salt content than N2, yet the floes appear similar in the surface photographs.

Appendix A contains diagrams of the floe samples. The sparse snow cover and deep frazil layers correspond well with core data reported by Ramseier et al (1974) and Gloerson et al (1974) during the Bering Sea Experiment (BESEX). Taken further north in an area where the ice advected southward, these cores show thick, white, snow-covered ice and areas of grey ice forming in leads downwind from the polynya south of St. Lawrence Island. Appendix A also shows a diagram of a typical thick white ice core and a grey ice core from each study for comparison, and indicates that this is not an anomalous ice situation.

4.2 Davis Strait Ice Conditions

Documentation on ice conditions in Davis Strait comes from several sources, but extensive ice core data do not exist due to the extreme melt conditions encountered at the edge. Livingstone et al (1981) report an air temperature of 0°C and an ice surface temperature of -2°C for the flight. Gray et al (1979) discuss the two ice cores taken for the period. The helicopter could not land on the ice, but hovered above the floes while researchers retrieved the samples. They state that the snow surface was dry, but the snow-ice interface was wet. The Ph-value and salinity indicate melting ice with salt water intrusion. Appendix A also contains their schematic diagram of the floes sampled.

In the study area, the floe size increased away from the ice edge ranging from 5-10 m at the edge to 10-30 m further in, and ending in a region of 2.2 x

2.8 km large floes (Gray et al, 1979; Livingstone et al, 1981) also observed this change in floe size on the airphotos taken. The large floes appear to be refrozen pancake ice or breccia with rough surface texture. The ice edge is less diffuse than the conditions encountered in the Bering Sea (figure 31). The ice edge appears compact and the floes at the ice-wate. boundary decrease in size by melting in situ. Some ice bands existed (figure 32) but do not show the active floe herding apparent in the Bering Sea (figure 14). Wave-broken white ice floes dominate the floe types while the grey-white floes apparent in the Bering do not exist in large amounts. Some lightly snow-covered nilas or grey ice occurs further into the flight line and seems to be formed from local re-freezing of open water areas within the white ice floe matrix (figure 33).

Ketchum and Farmer (1980) mention the general ice conditions found during the overflight of the NORDA P3. They state that the ice fields increased in size and extent from the Baffin Bay area to Davis Strait. The ice cover had a high density, but low surface relief with ridges usually less than 1 m high. Multiyear ice from the Canadian Archipelago and Nares Strait appeared but neither consistently nor in large amounts. However, icebergs, bergy bits and growlers from Greenland glaciers are common. Ketchum and Farmer agree that the edge consisted of swell broken floes with larger floes away from the ice edge. They describe the larger floes as consisting of some refrozen breccia and some flat ice. Most of the ice types encountered were thin first year or young ice and the nilas present was snow covered. The thickest snow cover occurred in the northwest portion of the line and appeared to be recent. The surface temperature the day before was +4°C, well above the freezing point. The PRT 5 data indicates that the surface temperature of the snow, water and ice were nearly isothermal at 0° to -1°C, indicating advanced melt conditions.

The shape of the ice edge and the few ice bands leads to the assumption that southerly winds exposed the ice to warmer temperatures and compacted the edge, and that melt conditions continued at the time of the overflight, but with little or no wind.

4.3 Comparisons of Data Results

This section compares the active and passive microwave results from Davis Strait and the Bering Sea. In the following section 4.3.1 discusses the temperature effects on the snow and ice; section 4.3.2 contains the passive data and compares the scatterometer data to the radiometer results; and section 4.3.3 describes the X Band radar results.

4.3.1 Snow and Temperature Effects

Research conducted on ice in cold regions, such as the central Arctic pack, assumes that microwave measurements are unaffected by snow. When the snow is very cold and dry the air pockets and crystals in the snow do not significantly influence the microwave return (Weeks and Ackley, 1982). Central Arctic research also shows that the penetration (skin depth) of microwaves in the ice increases with increasing thickness. Since the brine in its upper layers effectively lowers the brightness temperature, young ice with a small skin depth has a low emissivity and surface scattering dominates. Older ice also has a low emissivity but, since the brine has drained out of this ice, the lower measurement derives from volume scattering due to the increased skin depth. The emissivity for different ice types increases with thickness until it reaches a maximum at 1 m for first year ice, then it decreases (figure 34). Data in the MIZ suggest that both surface and volume scatter in young ice contribute to the ambiguities in the signatures once ice melt begins.

For the outer zone of the MIZ, temperature effects on the ice dominate the returns for both active and passive microwaves. This holds true for the diffuse ice edge found in the Bering Sea, and the compact ice edge found in Davis Strait. In summarizing all their data results, Livingstone et al (1981) describe several different temperature regimes and their effects on the ice and microwave data. Two of these apply to the MIZ. The intermediate zone ranges from -20°C to -3°C with the following changes noted: brine volume increases with increasing temperatures; surface scattering dominates in young ice types as the temperature increases, with the youngest ice classes affected first; the backscattering coefficient increases with increasing temperature as does the angular dependence; the emissivity decreases with increasing temperature. The following characteristics define the high temperature case ($T > -3°C$): surface water appears; surface scattering dominates; backscatter and emissivity decrease; and the Livingstone feature space classification breaks down, so that at some undefined temperature, microwaves will no longer discriminate ice types due to the dominance of surface water. Ambient temperatures define the ice cases used here, including Davis Strait, while the Bering Sea data include ice surface, air and water temperature. The results from the Bering suggest that effects ascribed to the higher temperature case also occur at lower ambient temperatures $> -6°C$ and at ice temperatures $\sim -5°C$ suggesting a lowering of the boundaries for the temperature criteria. The low air temperature does not account for the degree of ice melt found here and infers that the critical factors governing ice surface changes in the outer MIZ appear to result from melting induced by warmer sea water. More information needs to be obtained to evaluate the importance of water temperature as a criterion in ice signature identification for the MIZ.

Skin depth calculations for several frequencies combined with ice core results indicate that most microwave interactions in the Bering Sea occur in the frazil layer, but other factors suggest that snow effects are critical for the passive case since two different brightness temperatures exist for both grey-white and white ice. These appear to be related to a melting snow cover. The high return for the grey-white ice and the lower return of the white ice associated with the leading edge of an ice band confuses the ice signature separation for the classes. The effects of snow cover are unknown and warrant further investigation in the MIZ.

4.3.2 Radiometer and Scatterometer Data

Several investigators calculate skin depths for grey-white and white ice types at different frequencies. Livingstone et al (1981) estimate the skin depth for white ice at 19.35 GH_z under melt conditions to be less than 5 cm. For 10 GH_z Bogorodsky and Kukhov (1975) and Vant et al (1974, 1975) calculate skin depths for Bering Sea ice. Bogorodsky and Kukhov reported brine volumes and emissivities similar to N1 and show a skin depth of 2.4 cm for grey-white ice. The brine volume for frazil ice studied by Vant et al corresponds to N2 and yields an effective skin depth of 4.3 cm. They also report that the skin depth for columnar ice is larger at 11.5 cm. In data analyzed by Vant (1976) skin depths of 7.2-9.4 cm exist in ice at 7.5 GH_z under warm conditions. The lower frequency of the 6.6 GH_z radiometer gives a larger skin depth, but ice cores reported by Martin and Kauffman (1979), Ramseier et al (1974), and Gloerson et al (1974) indicate that for the frequencies studied, all interactions essentially take place in the frazil layer. Crystal sizes and brine pockets seen in the core photographs taken by Martin and Kauffman suggest that they are large enough to interact with the microwaves since they

are one-tenth the size of the measured wavelengths (Weeks and Ackley, 1982). This further reduces the skin depth of the ice providing additional evidence that the interactions take place in the frazil layer. Snow effects are unknown, but the high salinity and temperature of the snow, especially at the snow-ice interface, indicate that this layer could act as a reflective surface under melt conditions.

Grey-white ice in the Bering Sea shows two different emissivities in ice that appears similar on the photographs. The wet-surfaced ice has an emissivity of 0.71, somewhat lower than the measurement in Davis Strait. Some grey-white floes appeared to have a drier surface and had higher emissivities of 0.73. The white ice emissivities (0.72) are within the standard deviations of those found for grey-white ice, and fall below the reported measurements for Davis Strait. Ice in Davis Strait classifies by emissivity alone, but variations exist in similar ice types as a result of temperature effects (Livingstone et al, 1981). In the Bering Sea brightness temperature variations appear on different runs and within the categories defined by the ice cores. The mean values for all types varies from line to line with the mean for all samples being 198.2°K for grey-white ice and 203.4°K for white ice. These values fall within the standard deviations for the two classes and make them inseparable by brightness temperature or emissivity. Livingstone reports values of 229.1°K for rotten first year ice and 214.6°K for wave-broken first year ice at the edge. Both values seem to correspond to the white ice identified in the Bering Sea; a decrease in brightness temperature as a function of frequency is expected (Gray, 1980).

For both the Davis Strait and the Bering Sea, the grey-white ice shows large variations in brightness temperature with no apparent change in the ice visible in the photographs. For the Bering Sea the variation is ~30°K; for

Davis Strait, Livingstone comments that it is ~20°K. Taken individually, the brightness temperatures for these grey-white floes are quite high, but within the returns noted for white ice. These anomalies occur frequently enough that the higher temperatures skew the data for grey-white ice as a whole, confusing it with the white ice returns. Figure 35 shows radiometer and scatterometer (θ=58°) data for a bright grey-white ice occurance (the peak seen in the area marked 2 on the figure). The scatterometer fails to resolve the ambiguity in the brightness temperatues, indicating that at this angle, the surface of the two ice types appear similar. As the snow begins to melt on the ice, small water droplets form in the snow before the surface appears wet. These droplets enhance the brightness temperature of the ice compared to dry unmelted snow, and wet snow found on other floes (see inset, figure 35). The water in the snow in both melt cases creates a reflective layer for the scatterometer and explains the difference in the ability of the sensors to discern the brighter ice type.

In some cases, white ice floes also give lower returns than expected. This often appears as a decrease in brightness temperature at the ice edge, or at the leading edge of an ice band (figure 36). Livingstone reports similar effects. In the Bering Sea data, a tendency exists for a slight rise in backscatter associated with this decrease. Livingstone's data also indicates this rise, but to a lesser degree (figure 37). Martin et al (1983) report that ice at the leading band edge has more freeboard, and a drier surface compared to the trailing edge. The inset in figure 36 shows a schematic diagram of the initial ice band appearance (a) and decay (b) with time. For both cases, thicker, rougher ice exists at the leading edge. Core N2 (figure A-2), taken at the edge of an ice band, shows the low salinity associated with this ice. The dry surface with little brine in it causes volume scattering to

dominate in this case, lowering the brightness temperature while the drier, rougher surface relief enhances the scatterometer return. The Davis Strait ice edge contains remnant, thicker floes. Their advanced state of decay and lesser degree of rafting due to wind conditions combine to give the smaller increase in backscatter. This is consistant with Livingstone's comment that due to surface roughness at the cake edges, wave-broken ice at the edge has a slightly higher backscattering coefficient than unbroken, rotting ice in Davis Strait. The wet snow surface here is four times the depth of the drier Bering Sea ice (figure A-4) so that surface moisture accounts for the dramatic decrease in brightness temperature instead of volume scattering.

The two studies also show an increase in brightness temperature in footprint samples taken in open water before contact with the ice edge. The open water signature occurs most often at the leading ice edge. The trailing ice edge often contains secondary peaks where the footprint encounters an ice-water mixture. Figure 38 shows these conditions for an ice band in the Bering Sea. Area 1 contains grey-white ice; 2 has white floes associated with the leading edge of a band; 3 contains mixed ice types. Area 4 shows the secondary peaks associated with the low-concentration floes in the trailing edge of a band, while 5 indicates the open water areas associated with the increased brightness temperature on approaching the ice edge. The reason for this increase is not understood.

Problems exist in combining the scatterometer data with the airphotos and the radiometer data. Time code errors eliminated two minutes of data on each five minute run. Low altitude passes prevented overlap on the airphotos. These factors combined with the loose ice conditions and angle changes on the scatterometer every 5 s on some runs left few areas where all three data types existed simultaneously. The best data exists where there is a fixed angle on

the scatterometer allowing sufficient sampling so that one ice type fills the footprint, in this case at θ=58°.

Figure 38, a plot of emissivity (ε) and backscatter for run 11-0 shows that the two ice types are inseparable under these conditions. The mean emissivity and backscatter plotted with their error bars suggest some separability, but the previously mentioned problems in defining ice type by emissivity and the variations of emissivity in different lines leaves backscatter to define the classes, and these values overlap considerably. Figure 35, shown previously, indicates the non-separability of ice types by backscatter since a clear difference in the ice types exists here. Data taken by Livingstone et al (1981) in the Beaufort Sea and Frobisher Bay show the return in Davis Strait to be more specular. They indicate that first year and grey-white ice categories separate only at θ=8° to 18°. For θ=58°, the two cases are inseparable, though the possibility exists that Bering Sea data may separate at smaller angles. The amount of surface water present may cause this specular relfection and breakdown of the separability. This implies a change from volume scattering to surface scatter with an increase in the surface water layer.

4.3.3 Radar Data

This sub-section compares X Band radar data taken in the Bering Sea and Davis Strait. Cores in Davis Strait contained more snow, and environmental conditions exist for more snowfall during the ice season (Maxwell, 1981; Crane, 1978). Ketchum and Farmer (1980) indicate that wet snow increases the backscatter on X Band but not L Band radar returns from Davis Strait. The differences derive from the amount of slush cover present. Slush cover gives a lower return than a melting snow cover. This apparent increase makes the

X Band data ambiguous, and necessitates using X and L Band together to resolve the data. Snow on very thin ice gives a high return on X Band, low on L Band, while thin ice without snow is low on both X and L Band.

Ice band structures in the Bering Sea consist of small, consolidated ice forms, pieces which cannot be individually resolved on X or L Band data (Ketchum and Farmer, 1980). However, X Band gives a higher return for melting snow, and floes in an ice band provide excellent discriminators for ice features at the edge (figure 40). Data from the C131 X Band radar shows that it resolves the features well at both near and far range. Ketchum and Farmer (1980) state that the homogeneous grey tone of the ice seen near the edge results from a high density of surface scatterers and reflection at an interface boundary. Figure 41 shows a portion of the ice band labeled A on figure 40 and shown in detail in figure 41, and indicates the ability of the radar to image these features regardless of frequent cloud cover. The location and condition of the ice at the ice edge responds to changes in meteorological conditions, and radar imagery is useful in predicting ice edge motion. Area B on figure 40 shows lead orientation patterns in the active ice zone to the east of St. Lawrence Island. Ice from Norton Sound, and thick ice from the northern Bering Sea advects through this area at speeds as high as 34 cm s^{-1} (McNutt, 1981). Such ice presents a hazard, and shifts in the lead orientations precede changes in the polynya locations and ice thickness distributions for the entire basin.

Ketchum and Farmer also report that fast ice fragments can be discriminated on X Band data due to the contrast with the first year ice matrix. X Band data taken 27 March 1979 in Norton Sound, figure 42, show the onset of ice retreat in the area. The fast ice marked C on the image, gives different returns in two areas. C1 differs from the first year ice near it

due to ridging on the mobile ice, but C2, broken off from the fast ice north of St. Lawrence Island and advecting northward with the pack, shows no difference from the surrounding ice. Its surface may be wet causing the more specular return. Figure 43 shows the TIROS image for 25 March, 26 and 27 March being too cloudy to show ice detail. Thus, the radar discriminates ice from open water and shows ice concentration better than the visual image.

5.0 Conclusions

The Bering Sea and Davis Strait data suggest that temperature effects dominate the active and passive microwave returns collected under melt conditions in the MIZ. Specifically, the conclusions address the following considerations:

1. The ice classification scheme of Livingstone breaks down at ambient temperatures <-3.0°C, and Bering Sea data suggest water temperature influences ice returns more than air temperature within a certain range in the outer zone of the MIZ.

2. Snow cover effects are unknown, yet appear to influence the returns significantly under melt conditions.

3. Skin depth calculations combined with ice core reports, discounting the snow cover, indicate that most interactions at the microwave frequencies studied take place in the frazil ice layer.

4. Two different conditions existed in the MIZ: the diffuse edge case in the Bering Sea; the compact edge case in Davis Strait. The data collection scheme used in Davis Strait suits both conditions better than the design used in the Bering Sea. An analysis of Bering Sea ice processes suggests that regions to the east of St. Matthew Island better represent the ice, as a whole, in the Bering basin.

Livingstone et al (1981) state that the ice classification scheme breaks down with increasing temperatures as the surface scatter from meltwater dominates the returns, the critical temperature being -3°C. Lower temperatures existed in the Bering Sea with surface effects already apparent, suggesting that the classification breaks down at temperatures lower than -3°C if the ice encounters warm water. Since the ice edge limit in the Bering Sea depends on the location of this warmer water, water temperature may play a

greater role in governing the breakdown of ice signatures in the MIZ than the ambient air temperatures over a limited range. The difference in the ice appearance under melt conditions also suggests a strong need to understand the morphology of the ice at the edge where ice with a large frazil layer and little snow cover melts more rapidly than rafted ice which is thicker.

Snow cover also affects the growth rates of ice, and the free water content of the melting snow may contribute to ambiguities in the microwave return. The radiometer and scatterometer data collected for Davis Strait and the Bering Sea do not address the problems of snow accumulation and changes in the snow cover during melting. Increases in brightness temperatures and reflectivity of the surface water layer suggest that snow cover must be considered in future identification schemes in the MIZ.

The results at all frequencies in the Bering Sea indicate that interactions take place essentially in the frazil layer. The emissivity and brightness temperatures for the two ice types encountered failed to identify the ice, unlike the situation in Davis Strait. Both brightness temperature and the scatterometer return at $\theta = 58°$ could not distinguish the two types of ice found. The increase in the brightness temperature of the water near the ice edge is not understood. Ice at the leading edge of an ice band and at the ice edge under compact ice conditions both show a decrease in brightness temperature as the footprint approaches open water. In one case this may be due to volume scatter, and in the other, surface scatter from meltwater. In the first case there is a stronger increase in backscatter associated with the decrease in brightness temperature and this may be helpful in resolving the different processes involved. The limited data set here warrants further investigation. A deficiency in the data collection system used did not generate enough scatterometer information at angles $< 58°$. Since the best

data existed where the angle held constant for a run, this method should be applied in diffuse ice conditions where data cannot be collected at all angles simultaneously as on the CCRS scatterometer.

The location of satellite tracks determined the ship's station for data collection in the Bering Sea. The area behind Nunivak Island exhibits regional ice characteristics which may not represent the majority of the thicker pack ice in the Bering Sea which migrates to the ice edge. Although the floe samples are similar to the BESEX floes taken further west, these may also be from the downwind end of a polynya region, in this case behind St. Lawrence Island. A more suitable study region exists above the level shelf area to the east of St. Matthew Island where thicker ice advects to the edge from the north-northwest (McNutt, 1980). A ship-borne helicopter provides necessary scientific support for collecting ice samples at the ice edge and further into the pack. Accurate determination of the microwave ice properties necessitates this support as airphotos alone do not provide completely reliable information on floe characteristics, e.g., the normal appearance of the bright grey-white floes.

A more optimal data collection design consists of long runs over the ice taking care to have all instruments and the camera tied to the main clock on the inertial navigation system, with a back up time code included. The nature of the MIZ precludes stepping through scatterometer angles or constantly changing the data collection mode on any sensor, especially with diffuse ice conditions. Longer runs into the ice with fixed angles and with similar ice conditions give more valid ice samples and provide signatures for the ice forms found at the edge which have not yet encountered melt conditions. Longer runs also aid in radiometer and scatterometer comparisons. Flightlines long enough to encounter fast ice and ice in polynyas would be ideal, if logistically feasible.

The cameras used by CCRS and NASA differed significantly. The wide angle lens of the CCRS camera showed more area, but at a cost in resolution which might affect an understanding of the surface of the ice and the amount of water and different ice types actually present in the sampling footprints. Radar provides a better wide area indication of ice conditions while the 6" focal length lens of the NASA camera gives more accurate information on the surface condition of the ice and correlates better with surface photos taken on the ice floes. Flightlines must be planned so that the lowest critical altitude for data collection provides overlap of the images to produce photo mosaics. An imaging radiometer and/or IR onboard facilitates data analysis and provides better monitoring of processes and morphology in the area.

Finally, the data indicate two different ice edge scenarios for the MIZ. In order to accurately compare ice signatures for both geographic regions, investigators must plan for an experiment which lasts long enough to encounter both diffuse and compact ice edge conditions. Changes in wind and wave climatology drastically alter the ice conditions and create different effects on the surface properties of the ice involved. Monitoring the ice as it changes, with ground truth taken before and after the meteorological events, may resolve some of the questions concerning ice processes and their relationship to the changes in ice signatures in the MIZ.

Acknowledgments

This work was performed under NASA contract NAG 5-161, and JPL contract 45-646-40015-0-3260. I thank Dr. Seelye Martin of the School of Oceanography, University of Washington, for his assistance during the last 2 years and for advice on ice edge properties. Drs. Rene Ramseier of the Atmospheric Environmental Services, Ottawa and Frank Carsey of the Jet Propulsion Laboratory provided needed support at a critical time. I also want to thank Dr. Tom Grenfell, Atmospheric Sciences Department, University of Washington for discussions on the microwave data.

Bibliography

Bauer, B.J. and S. Martin, 1980, Field observations of the Bering Sea ice edge properties during March 1979, Monthly Weather Review, 108, 2045-2056.

Bogorodsky, V.V. and G.P. Kukhov, 1975, Electrical properties of ice in the ice edge zone of the Bering Sea at 10 GH_z frequency, USSR/USA Bering Sea Experiment, Proceedings of the Final Symposium on the Results of the Joint Soviet-American Expedition, May, 1975, Gidrometeoizdat, Leningrad, 219-232.

Coachman, L.K. and K. Aagaard, 1980, Reevaluation of water transports in the vicinity of Bering Strait, in: The Eastern Bering Sea Shelf: Oceanography and Resources, D. Hood and J. Calder (eds.), Government Printing Office, GPO, 95-110.

Coachman, L.K., K. Aagaard and R.B. Trip, 1975, Bering Strait: The Regional Oceanography, University of Washington Press, Seattle, WA, 172pp.

Collin, A.E. and M.J. Dunbar, 1964, Physical Oceanography in Arctic Canada, Annual Bulletin of Oceanography and Marine Biology, 2, 45-75.

Crane, R.G., 1978, Seasonal variation in sea ice extent in the Davis Strait and Labrador Sea, and its relation with synoptic scale atmospheric circulation, Arctic, 31(4), 434-447.

Crawford, J.P. and C.L. Parkinson, 1981, Wintertime microwave observations of the North Water polynya, in: Oceanography from Space, J.F.R. Gower (ed.), Plenum Press, NY, 839-844.

Dey,B., 1981, Monitoring winter ice dynamics in the Canadian arctic with NOAA-TIR images, Journal of Geophysical Research, 86, 3223-3235.

Dunbar, M., 1967, The monthly and extreme limits of ice in the Bering Sea, in: Physics of Snow and Ice, Proceedings of the International Conference, Sapporo, Japan 1966.

Dunbar, M., 1972, Increasing severity of ice conditions in Baffin Bay and Davis Strait and its effect on the extreme limits of ice, Proceedings of Sea Ice Conference, Reykjavik, Iceland, 87-93.

Dunbar, M., 1973, Winter regime of the North Water, Transactions of the Royal Society of Canada, series 4, v. 11, 275-281.

Fleet Weather Facility, 1978, Eastern-Western Arctic Sea Ice Analysis, Commander J.D. Langemo, C.O., Suitland, MD.

Fleet Weather Facility, 1977, Eastern-Western Arctic Sea Ice Analysis, Captain J.A. Jepson, C.O., Suitland, MD.

Fleet Weather Facility, 1976, Eastern-Western Arctic Sea Ice Analysis, Commander V.W. Roper, C.O., Suitland, MD.

Gloerson, P., Ramseier, R.O., Campbell, W.J., Chang, T.C., and T.T. Wilheit, 1975, Variation of the morphology of selected micro-scale test areas during the Bering Sea Experiment, in: Results of the U.S. Contribution to the Joint U.S./U.S.S.R. Bering Sea Experiment, NASA/Goddard (NASA X-910-74-141) 104-121.

Gray, L., Gudmandsen, P., Overgaard, S., Skou, N., and F. Søndergaard Pedersen, 1979, West Greenland Sea Ice Experiment, SURSAT Report No. 1, Electromagnetic Institute, Technical University of Denmark, Lyngby, Denmark.

Harrington, R., 1980, The Development of a Stepped Frequency Microwave Radiometer and its Application to Remote Sensing of the Earth, Dissertation, Old Dominion University, Norfolk, Virginia.

Hawkins, R.K., Gray, A.L., Linvingstone, C.E. and L.D. Arsenault, 1981, Seasonal effects on the microwave signatures of Beaufort Sea ice, Proceedings, 15th International Symposium on Remote Sensing of the Environment, Ann Arbor, MI.

Ito, H. and F. Müller, 1982, Ice movement through Smith Sound in northern Baffin Bay, Canada, observed in satellite imagery, Journal of Glaciology, 28(98), 129-143.

Jacobs, J.D., Barry, R.G. and R.L. Weaver, 1975, Fast ice characteristics with special reference to the eastern Canadian Arctic, Polar Record, 17(110), 521-536.

Jones, W.L., Schroeder, L.C., and J.L. Mitchel, 1977, Aircraft measurements of microwave scattering signatures of the ocean, IEEE, AP-25, 52-61.

Ketchum, R.D. and L.D. Farmer, 1980, Eastern Arctic SURSAT SAR Ice Experiment: Radar Signatures of Sea Ice Features, Naval Ocean Research and Development Activity (NORDA) technical note 68, 38pp.

Ketchum, R.D., 1977, An Evaluation of Side Looking Radar Imagery of Sea Ice Features and Conditions in the Lincoln Sea, Nares Strait and Baffin Bay, NORDA technical note 7, 30pp.

Kinder, T.H., 1980, Perspective of physical oceanography in the Bering Sea, 1979, in: The Eastern Bering Sea Shelf: Oceanography and Resources, v.1, D. Hood and J. Calder (eds.), GPO Press, 5-14.

Kinder, T.H., Coachman, L., and J. Galt, 1975, The Bering slope current, Journal of Physical Oceanography, 5, 231-244.

Livingstone, C.E., Hawkins, R.K., Okamoto, K., Arsenault, L.D., Pearson, D., Wilkinson, T.L. and A.L. Gray, 1981, The CCRS/SURSAT Active-Passive Experiment 1978-1980: The Microwave Signatures of Sea Ice Types and Features and their Implication for Remote Sensing, Canada Centre for Remote Sensing, Ottawa, in press.

Loshchilov, V.S., 1975, Characteristics of the ice cover in the operational area of the Bering Expedition, in: Preliminary Results of the Bering Expedition, pp. 18-30, (available in translation from NASA, Washington, D.C. 20546)

McNutt, L., 1981, Ice Conditions in the Eastern Bering Sea from NOAA and LANDSAT Imagery: Winter Conditions 1974, 1976, 1977, 1979. NOAA Technical Memo ERL-PMEL-24, Seattle, WA, 179pp.

McNutt, L., 1980, Remote sensing analysis of ice growth and distribution in the eastern Bering Sea, in: The Bering Sea Shelf: Oceanography and Resources, D. Hood and J. Calder (eds.), GPO.

Martin, S., Kauffman, P., and C. Parkinson, 1983, The movement and decay of ice edge bands in the winter Bering Sea, Journal of Geophysical Research, in press.

Martin, S., and P. Kauffman, 1979, Data Report on the Ice Cores Taken During the March 1979 Bering Sea Ice Edge Field Cruise on the NOAA Ship SURVEYOR, University of Washington, Department of Oceanography, Special Report, no. 89, September 14, 1979, 69 pp.

Maxwell, J.B., 1981, Climatic regions of the Canadian Arctic Islands, Arctic, 34(3), 225-240.

Muench, R.D., Tripp, R.B., and J.D. Cline, 1980, Circulation and hydrography of Norton Sound, in: The Eastern Bering Sea Shelf: Oceanography and Resources, D. Hood and J. Calder, (eds.), GPO, pp. 77-93.

Muench, R.D. and R.L. Charnell, 1977, Observations of medium-scale features along the seasonal ice edge in the Bering Sea, Journal of Physical Oceanography, 7(4).

Muench, R.D. and K. Ahlnäs, 1976, Ice movement and distribution in the Bering Sea from March to June 1974, Journal of Geophysical Research, 81(24), 4467-4475.

Newton, J. and B. Andersen, 1980, MIZPAC 80A: USCGC POLAR STAR Arctic West Operations, Science Applications, La Jolla, California, report SAI-202-80-460-LJ, 32pp.

OSCEAP, 1977, Climate Atlas of the Outer Continental Shelf Waters and Coastal Regions of Alaska, 2, Bering Sea, Arctic Environmental Information and Data Center, Anchorage, Alaska.

Overland, J.E. and C. H. Pease, 1980, Cyclone climatology of the Bering Sea and its relation to sea ice extent, Monthly Weather Review, 108.

Overland, J.E., 1980, Marine climatology of the Bering Sea, in: The Eastern Bering Sea Shelf: Oceanography and Resources, D. Hood and J. Calder (eds.), GPO, pp. 15-22.

Pease, C.H., 1980, Eastern Bering Sea ice processes, Monthly Weather Review, 108, 2015-2023.

Ramseier, R.O., Gloerson, P., Campbell, W.J. and T.C. Chang, 1974, Mesoscale description for the principal Bering Sea Ice Experiment, in: Results of the U.S. Contribution to US/USSR Bering Sea Experiment Greenbelt, MD, pp. 31-74 (NASA X-910-74-141)

Salo, S.A., Pease, C.H., and R.W. Lindsay, 1980, Physical Environment of the Eastern Bering Sea, March 1979, NOAA-PMEL Technical Memo, ERL-PMEL-21, Seattle, WA, 119 pp.

Schertler, R., 1979, Background information on copy negatives of LeRC original SLAR imagery, NASA/Lewis Research Center, Cleveland, OH.

Schumacher, J.D., Kinder, T.H., Pashinski, D.J., and R.L. Charnell, 1979, A structural front over the continental shelf of the eastern Bering Sea, Journal of Physical Oceanography, 9, 79-87.

Squire, V. and Moore, S., 1980, Direct measurement of the attenuation of ocean waves by pack ice, Nature, 283(24), 365-368.

Stringer, W.J., 1980, Nearshore Ice Conditions in the Eastern Bering Sea, Geophysical Institute, University of Alaska, Fairbanks, report ULAGR #278, 32pp.

Vant, M.R., 1976, A Combined Empirical and Theoretical Study of the Dielietric Properties of Sea Ice over the Frequency Range 100 MH_z to 40 GH_z, Ph.D. Dissertation, Carleton University, Canada, 462 p.

Vant, M.R., Gray, R.B., Ramseier, R.O., and V. Makios, 1975, Erratum: Dieletric properties of fresh and sea ice at 10 and 35 GH_z, Journal of Applied Physics, 46, p. 2339.

Vant, M.R., Gray, R.B., Ramseier, R.O., and V. Makios, 1974, Dielectric properties of fresh and sea ice at 10 and 35 GH_z, Journal of Applied Physics, 45, p. 4712-4717.

Wadhams, P. and V. Squire., 1980, Field experiments on wave-ice interaction in the Bering Sea and Greenland waters, 1979, Polar Record, 20(125), 147-158.

Webster, B.D., 1981, A Climatology of the Ice Extent in the Bering Sea, National Weather Service, Anchorage, Alaska, NOAA Technical memo, NWS AR-33, 38pp.

Weeks, W.F. and S. Ackley, 1982, The Growth, Structure and Properties of Sea Ice, NATO Advanced Study Institute on Air-Sea-Ice Interaction, Acquafredda di Maratea - 28 September to 10 October 1981, in press.

World Meteorology Organization, 1970, WMO Sea Ice Nomenclature, Geneva, Switzerland. [WMO/OMM/BMO - No. 259, TP145], 147pp.

Appendix A

This Appendix contains the ice report by Kauffman and Squire for 13 March 1979 and by Bauer for 14 March 1979. Table A-1 shows ice statistics for the cores N1 and N2 taken on 13 March, and for B5 taken 7 March. These compare with cores A3G, A3, and NW2. Ramseier et al (1974) report the first two and Gloerson et al (1974) recorded the third. Diagrams for these floes are in figures A-1 through A-3. The number above the schematic representation of the core (to the left of the graph) refers to the snow depth found; the number below the diagram indicates the total length of the core. Figure A-4 shows the ice core diagram as reported by Gray et al (1979) for Davis Strait.

Ice Reconnaissance 14 March 1979

Jane Bauer

1-5nm

Area where bands are forming approximately perpendicular to the wind. There are a lot of snow-covered cakes, most of which are rafted. At about 4nm there is an area of grey ice floes which are rafted. At about 4nm there is an area of grey ice floes which are larger than the surrounding snow-covered lakes.

6-8nm

There is much open water here with many rafted cakes floating loose.

8-20nm

There is a total mixture! Many snow-covered cakes, some rafted, but most fairly flat. There are also patches of grey ice. These floes are fairly large. The largest was about 700 yds by 400 yds. There are also patches of open water. About 20nm in, the open water had some grease ice streaks on it. As one progressed into the ice, the average floe size did increase.

(see figure 24)

Ice Reconnaissance 13 March 1979

Peter Kauffmann and Vernon Squire

ship: 58° 01.5' 166° 12.3'
course 350°

first floes 58° 02.1' 166° 12.0'
broken pieces of thick ice 10-20m in diameter 75% ice

58° 03.0' 166° 12.1'
ice changed to large floes of new ice (like N-1)
30-50 m diameter 80% ice

58° 04.2' 166° 12.5'
wide open water, 10 m diameter thick floes, 1% ice

58° 04.9' 166° 13.7'
N2 ice floes 10-30m across, thick and snow-covered, 80% ice

58° 06.0' 166" 15.3'
large thin grey floes with occasional thick floes (25%), 90% ice

Table A-1

	N1	N2	B5	A3G	A3	NW2
location	58° 06.8'N 166° 14.9'W	58° 05.7' 166° 13.2'	58° 49.3' 168° 44.8'	61° 58.6' 176° 04.0'	61° 58.6' 176° 04.0'	61° 29.5' 174° 58.0'
core length	205mm	600mm	340mm	255mm	640mm	410mm
frazil layer	130mm	330mm	300mm	135mm	160mm	360mm
columnar layer	75mm	60mm (rafted)	40mm	80mm	80mm (rafted)	90mm
snow layer	20mm	10mm	20mm	0mm	3mm	2mm
snow salinity	1.4%	0.7%	20.3%	--	--	--
surface scrape	18.2%	3.4%	18.9%	--	--	--
surface salinity	7.1%	2.2%	8.0%	<20%	5.1%	11.2%
surface temperature	-2.1°C	-2.4°C	-4.4°C	-12.4°C	-9.0°C	-4.4°C
brine volume	0.16%	0.04%	0.09%	0.09%	0.03%	0.13%

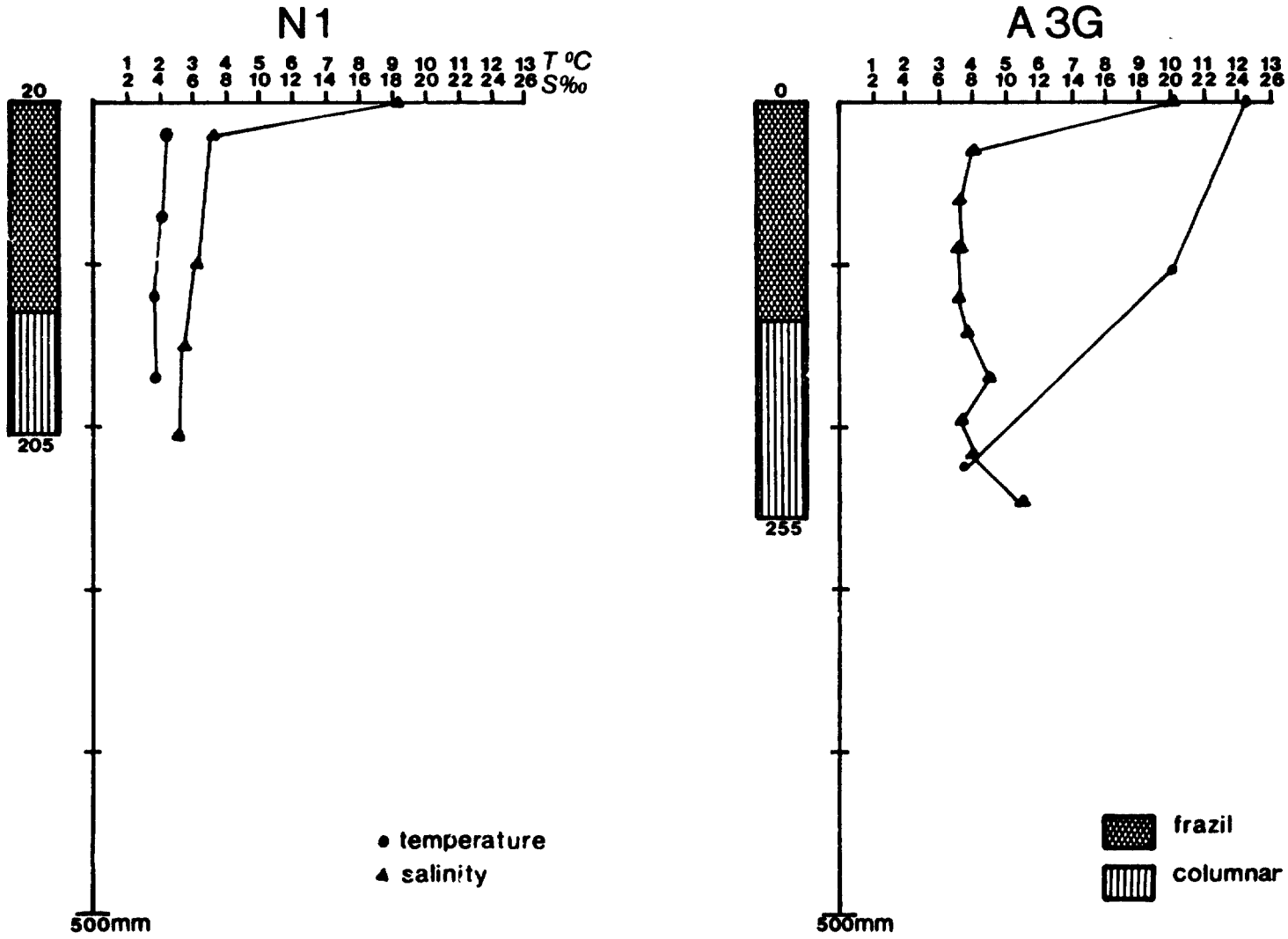

Figure A-1

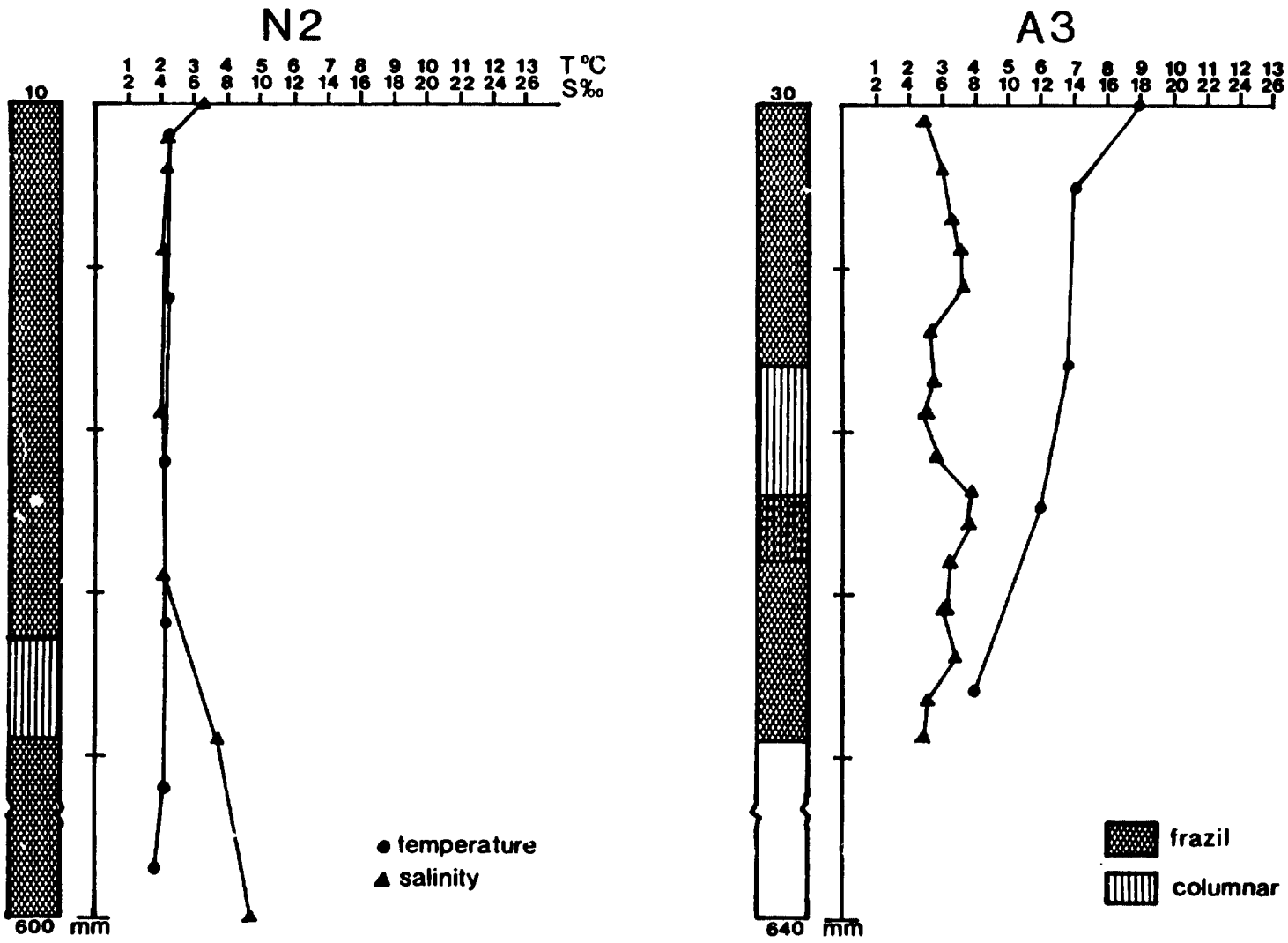

Figure A-2

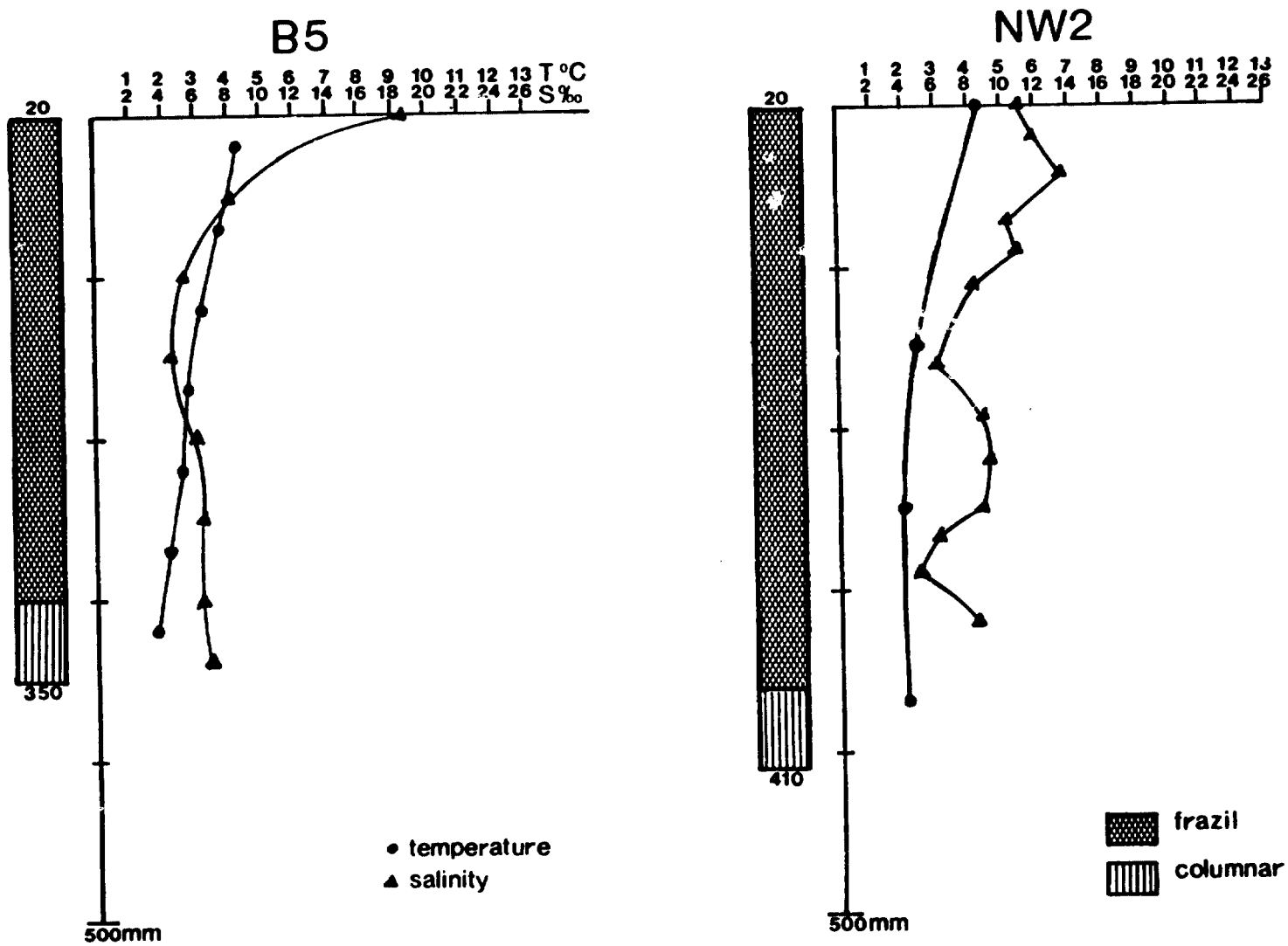

Figure A-3

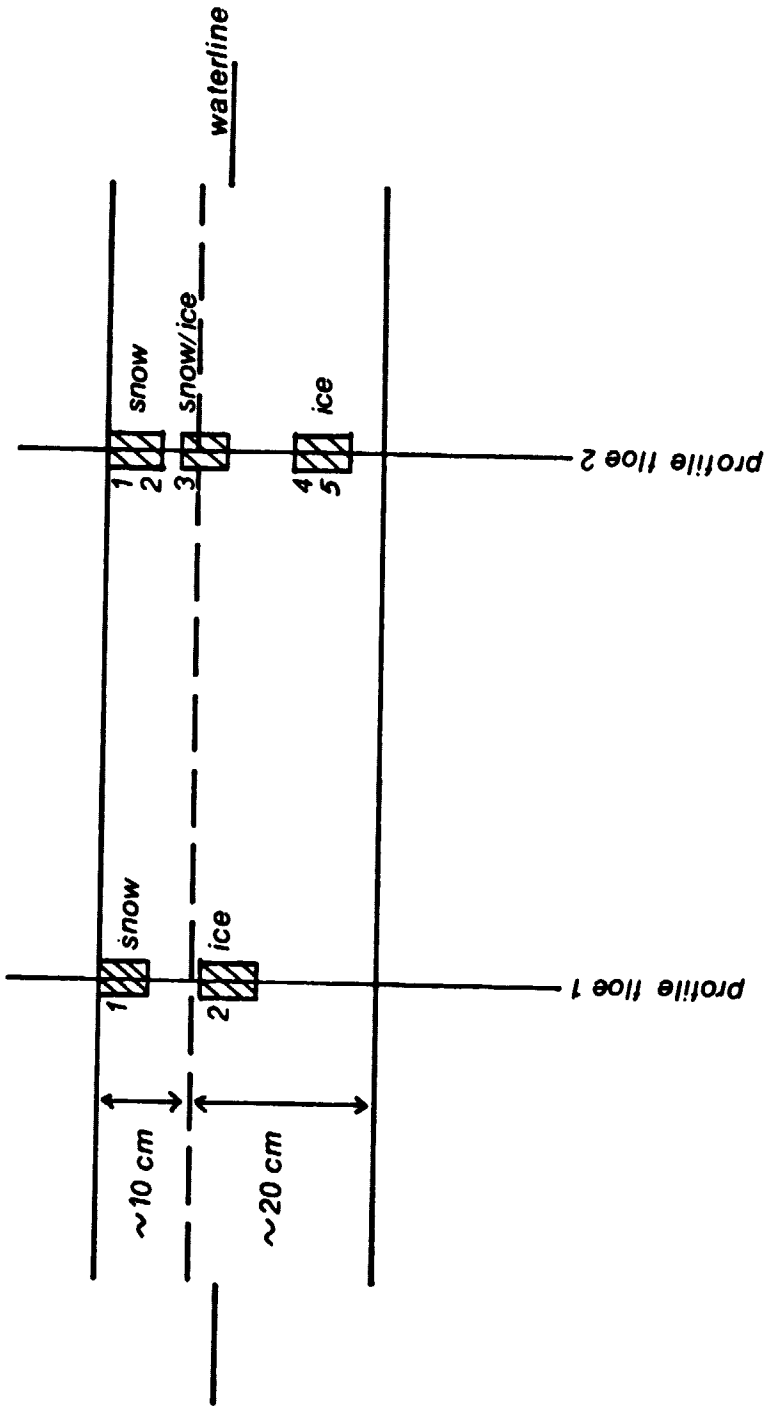

Figure A-4

List of Figures

Figure 9. Fast ice location for the Davis Strait region showing areas composed primarily of first year ice and those containing predominantly second-year and multiyear forms. (after Maxwell, 1981)

Figure 10. C130 flightline for 14 March 1979 in the Bering Sea.

Figure 11. Flightline for the CCRS aircraft 10 April 1979 in Davis Strait. (The other leg, from the north to the south, is not shown). (from Livingstone et al., 1981).

Figure 12. LANDSAT image from 13 March 1979 showing ice features in the Bering Sea: (1) fast ice north of St. Lawrence Island, (2) wedge of thick first year ice, (3) polynya on the leeward side of St. Lawrence Island where ice forms and advects downwind, (4) leads opening in pack ice as the ice diverges downwind, (5) ice bands forming at the edge.

Figure 13. Ice band showing two different ice types present. Note striations in the band and areas of wet, grey ice.

Figure 14. Ice band showing small ice floes moving downwind in the trailing edge of an ice band. The leading edge is in the lower portion of the photo and shows a well-defined ice/water boundary. The dark appearance of the middle of the mosaic results from changes in the automatic exposure of the photographs taken with the RC 9 camera.

Figure 15. Detail of the interior of an ice band showing the two types of ice present: (1) grey-white ice covered with snow, (2) grey-white ice with melted snow on a wet surface, (3) white ice floes appearing dry on the surface.

Figure 30. Ice core from floe B5.

Figure 31. Ice edge in Davis Strait. Compact ice conditions existed with little band formation; floe sizes increased away from the ice edge. (courtesy of C. Livinstone, CCRS)

Figure 32. Ice bands at the ice edge in Davis Strait. Compared to figure 14, little active herding of the floes by the wind exists, suggesting quiescent conditions. (courtesy of C. Livingstone, CCRS)

Figure 33. New ice formation inbetween white ice floes in Davis Strait. (courtesy of C. Livingstone, CCRS)

Figure 34. Microwave emissivity and ice thickness from the SURSAT active-passive experiment, 1979. Emissivity of Bering Sea ice generally is lower for grey-white ice with some samples correlating with the high emissivities found in the Beaufort Sea and Frobisher Bay ice. The emissivity of the first-year ice is significantly lower for the Bering Sea. In both cases, the surface conditions associated with melting explain the lower emissivity.

Figure 35. Brightness temperature vs. backscatter for the two ice types in the Bering Sea. (1) indicates thick white ice in an ice band. (2) shows grey-white ice. A large, snow-covered grey-white floe with little apparent surface melting created the spike in (2). Samples such as this occur frequently enough to skew the data and contribute to the difficulty in identifying the ice types. The scatterometer return ($\theta = 58°$) fails to resolve the different ice types. The inset shows a schematic representation of the free water in a partially melted snow surface, and its effects on emitted microwave energy.

Figure 36. The rise in backscatter and decrease in brightness temeprature associated with the white ice found at the leading edge of an ice band. The inset diagram shows a stylized representation of ice thickness in an ice band (a) as it initially forms, and (b) as it ablates downwind. In both cases thicker ice exists at the leading edge.

Figure 37. Backscatter and brightness temperature for wave-broken first year ice in Davis Strait. A slight tendency for a rise in backscatter with a decrease in brightness exists on approaching the ice edge. (from Livingstone et al, 1981).

Figure 38. Passive microwave data for an ice band in the Bering Sea: (1) grey-white ice, (2) white ice floes associated with the leading edge of a band, (3) mixed floe types, (4) the trailing edge of the band showing the secondary peaks associated with low-concentration ice floes, (5) the open water areas where the brightness temperature increases before the radiometer footprint encounters ice.

Figure 39. Plot of emissivity vs. backscatter ($\Theta = 58°$) for line 11-0 in figure 10. Emissivities and backscatter varied for different runs. In this case, the data appear separable, but the overlap makes identification difficult.

Figure 40. X Band radar imagery taken by the NASA C130 on 14 March 1979. Ice bands at the edge show up well due to the surface moisture. (A) indicates a large ice band seen in figure 41. The homogeneous return of the ice in the lower portion of the mosaic compares with the ridging and texture seen in the upper image taken further north; the difference arises from the change in the surface melt conditions from south to north.

Figure 41. Ice band seen in figure 40(A). The time difference between the two overflights accounts for the slight changes in the band shape.

Figure 42. X Band imagery mosaic for 27 March 1979 in Norton Sound. Areas C1 and C2 show fast ice. C1 has broken off from St. Lawrence Island and is advecting north with the pack ice. C2 is still fast off the coast near Nome. The dark return from the smooth ice in C2 distinguishes it from the surrounding ridged ice. C1 resembles the surrounding ice; its high return may be due to wetness on the surface.

Figure 43. TIROS image taken 25 March 1979 showing the ice imaged March 27 in figure 42. Both images show the open water, but clouds obscure the areas of mobile ice seen in figure 42. The TIROS image for 27 March was cloud-covered.

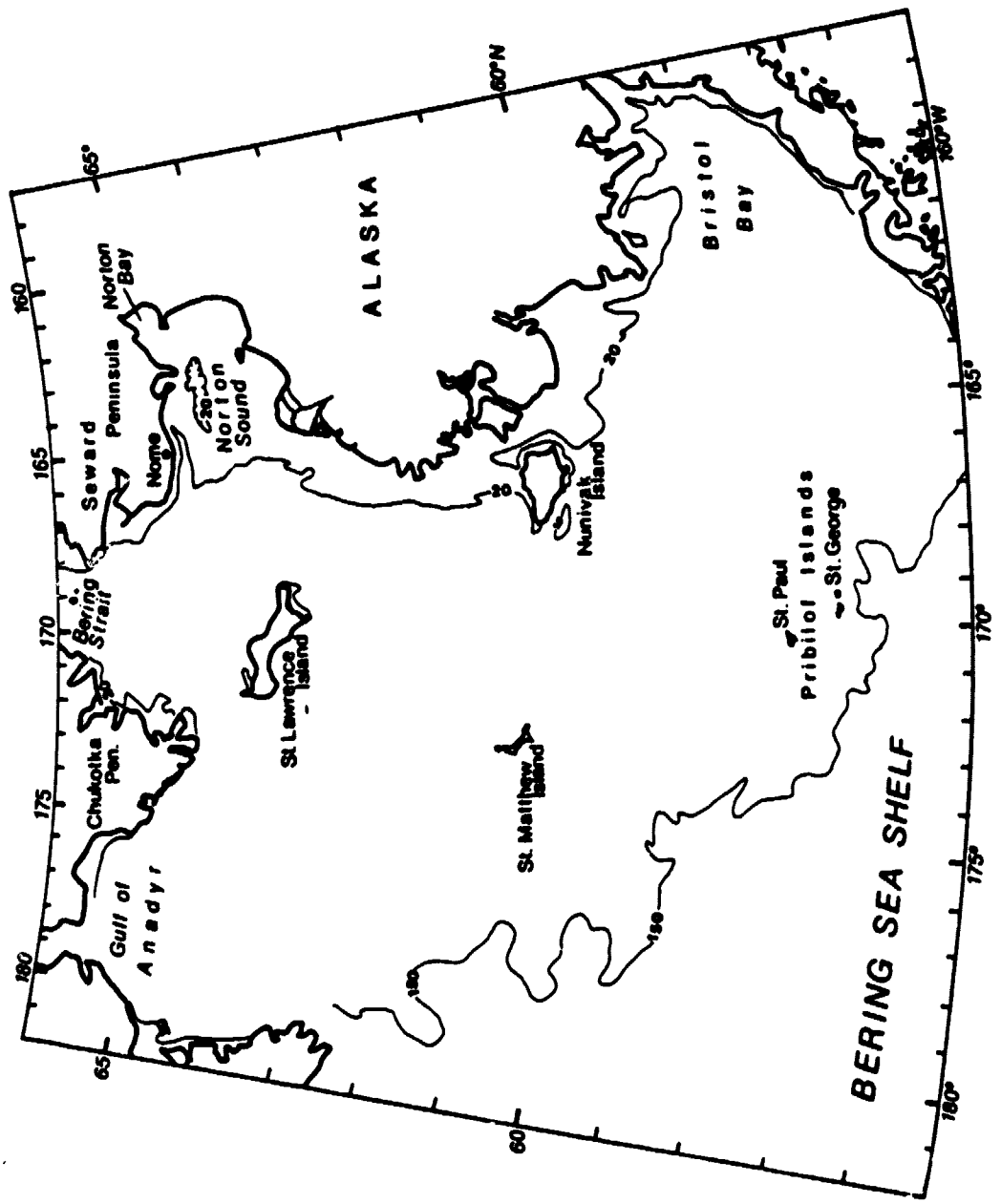

Figure 1

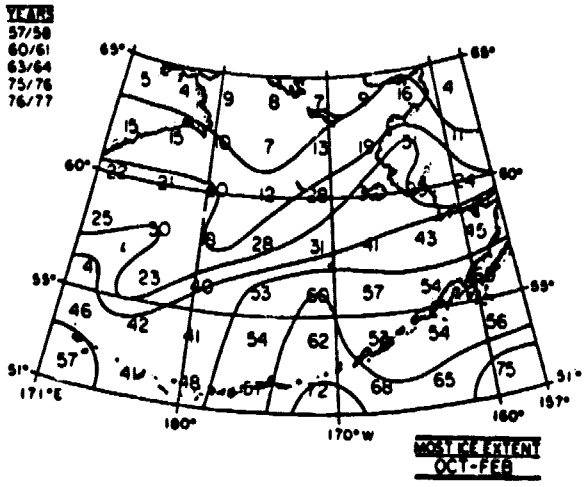

a

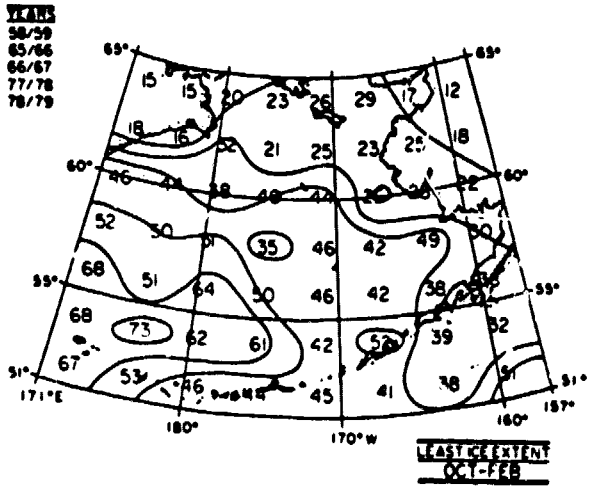

b

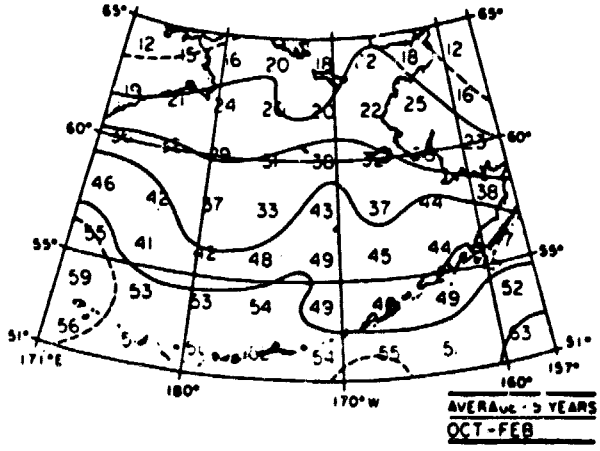

c

Figure 2

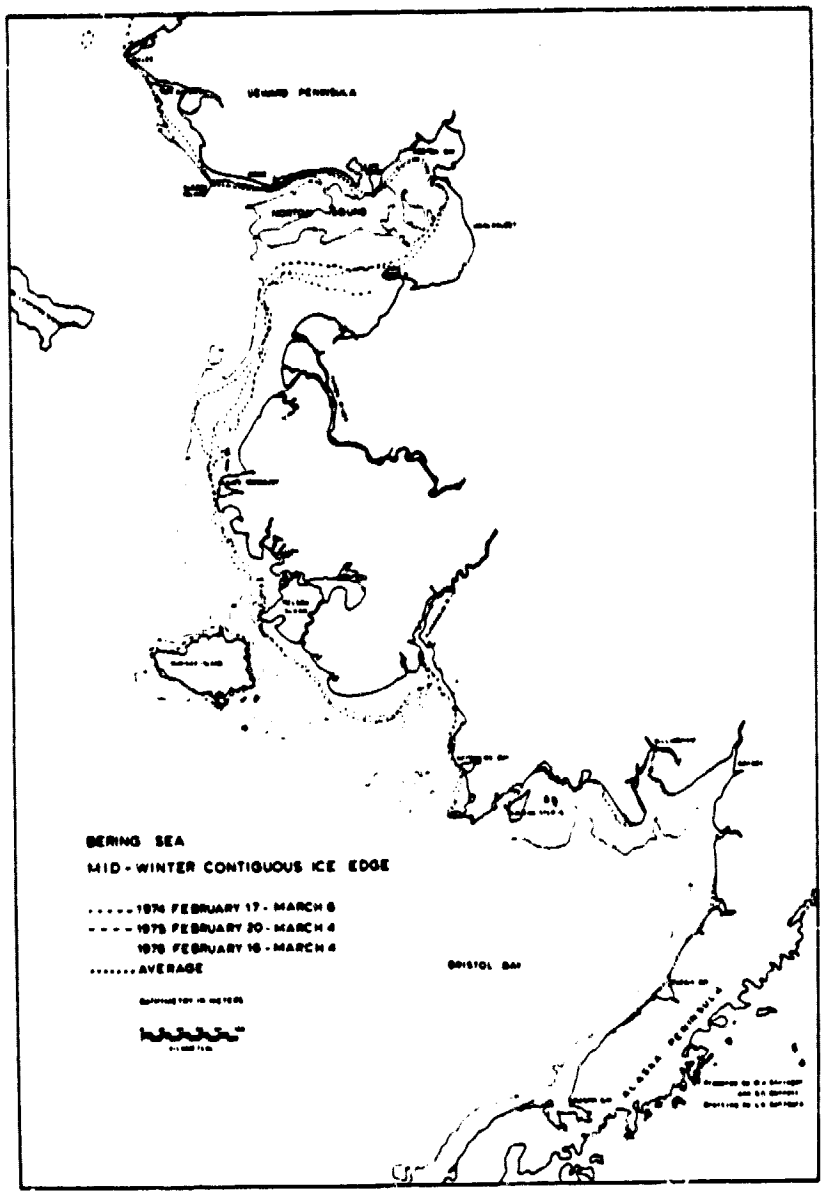

Figure 3

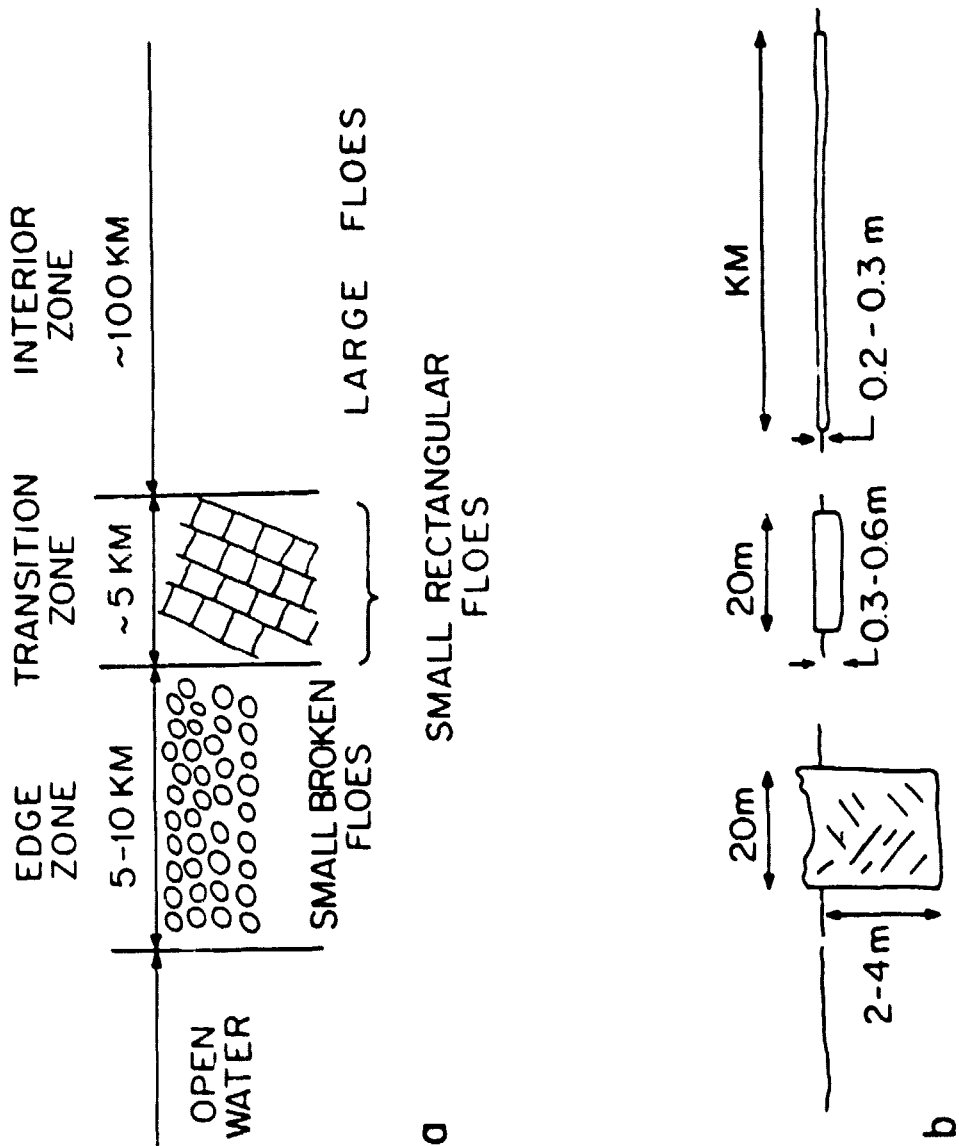

Figure 4

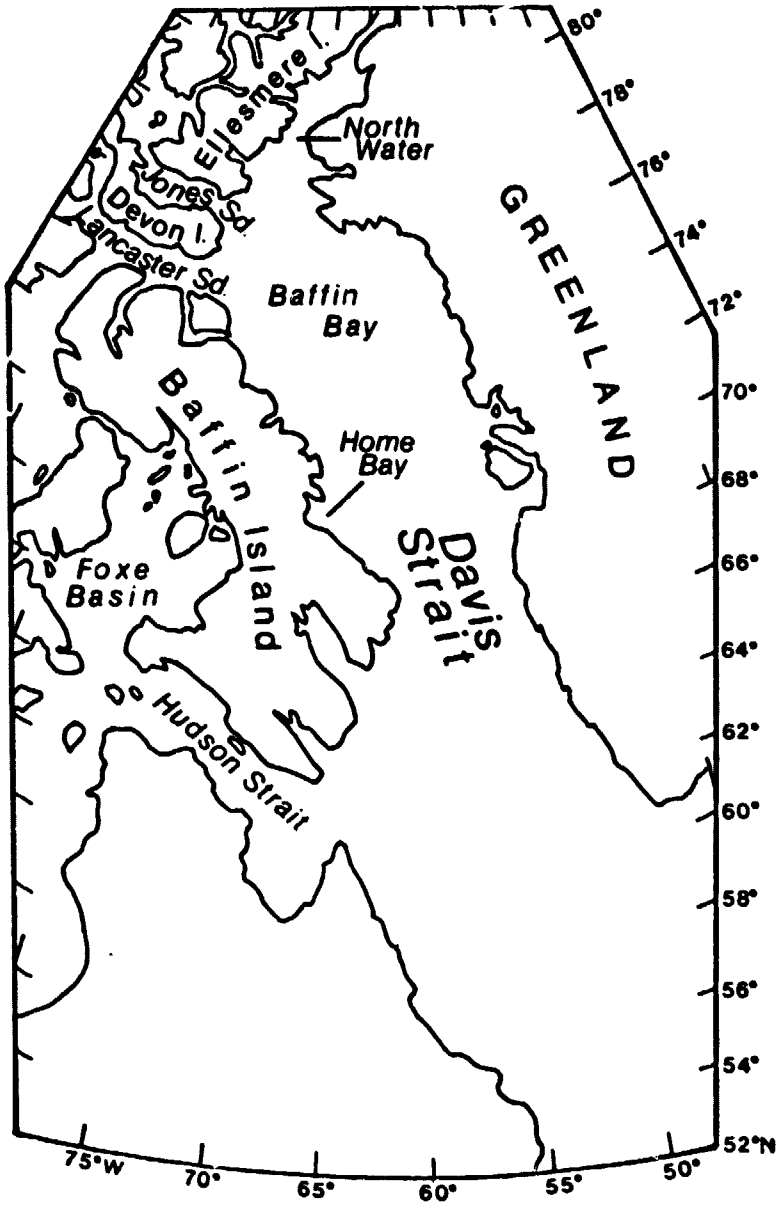

Figure 5

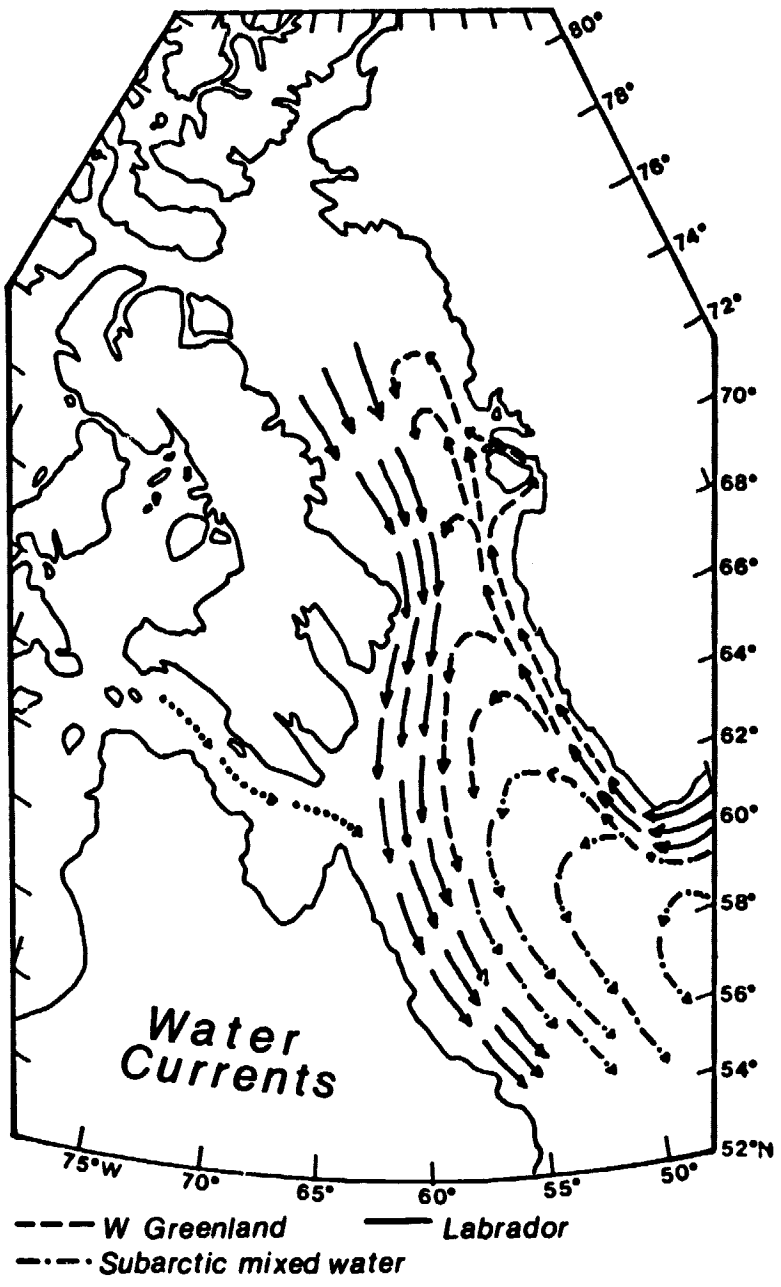

Figure 6

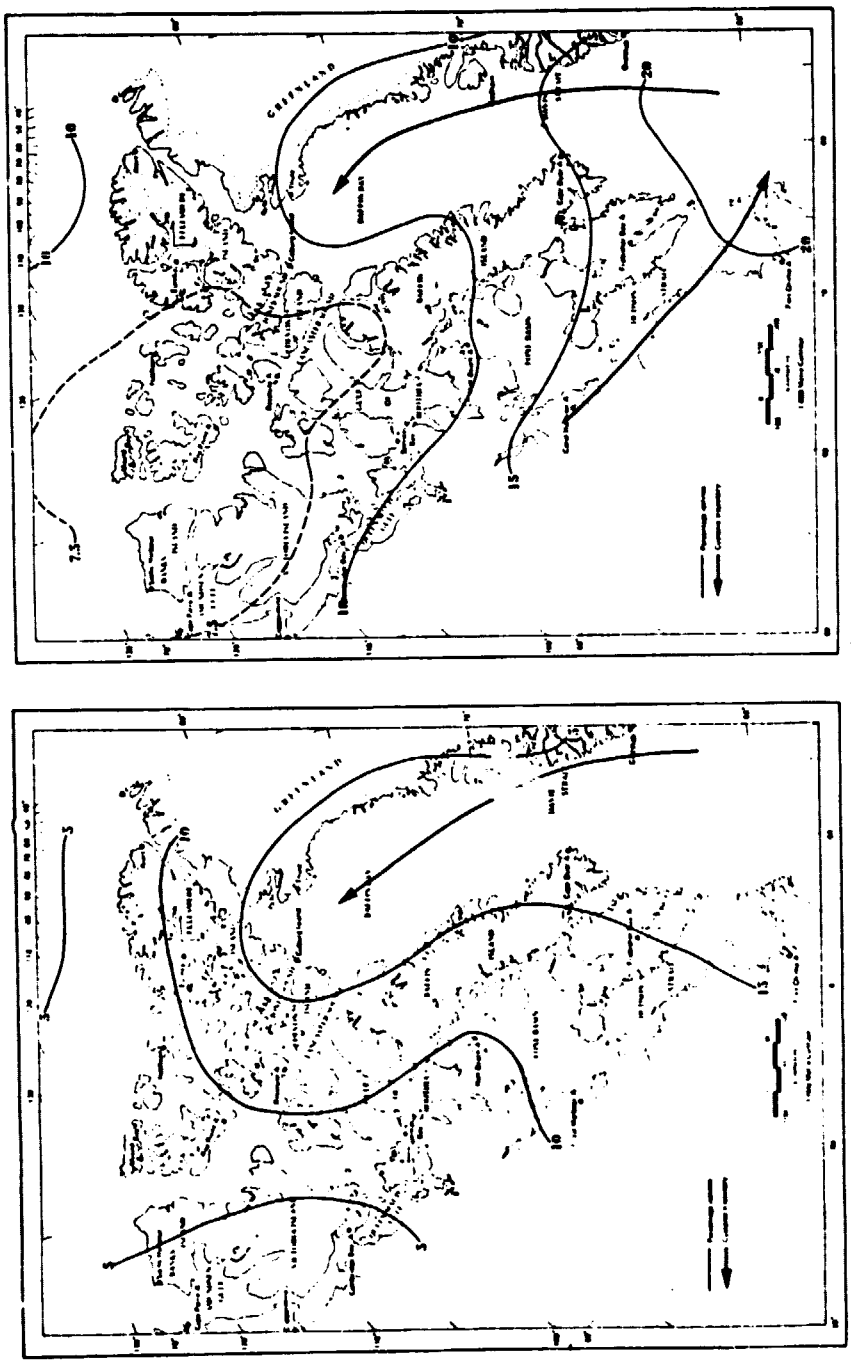

a b

Figure 7

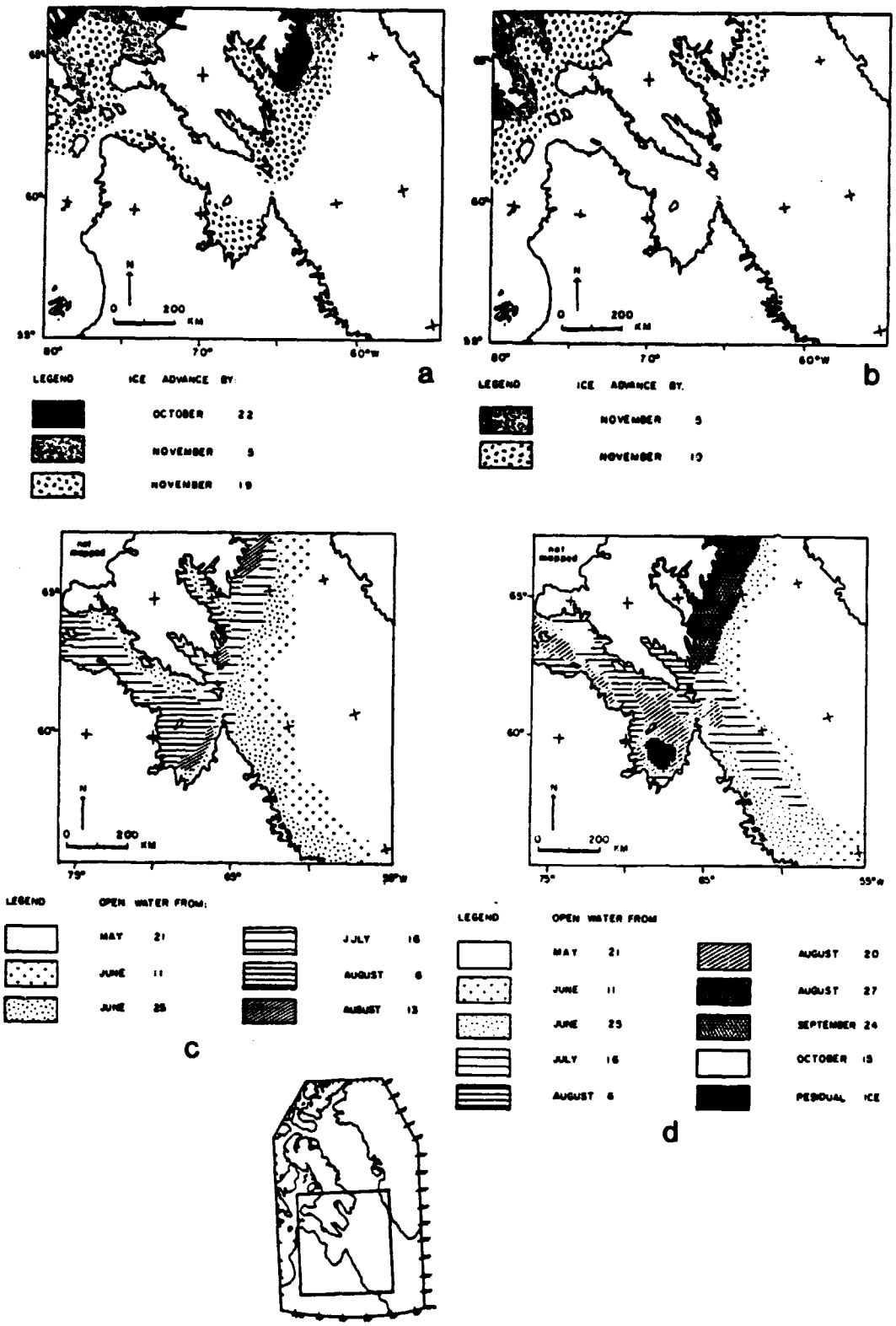

Figure 8

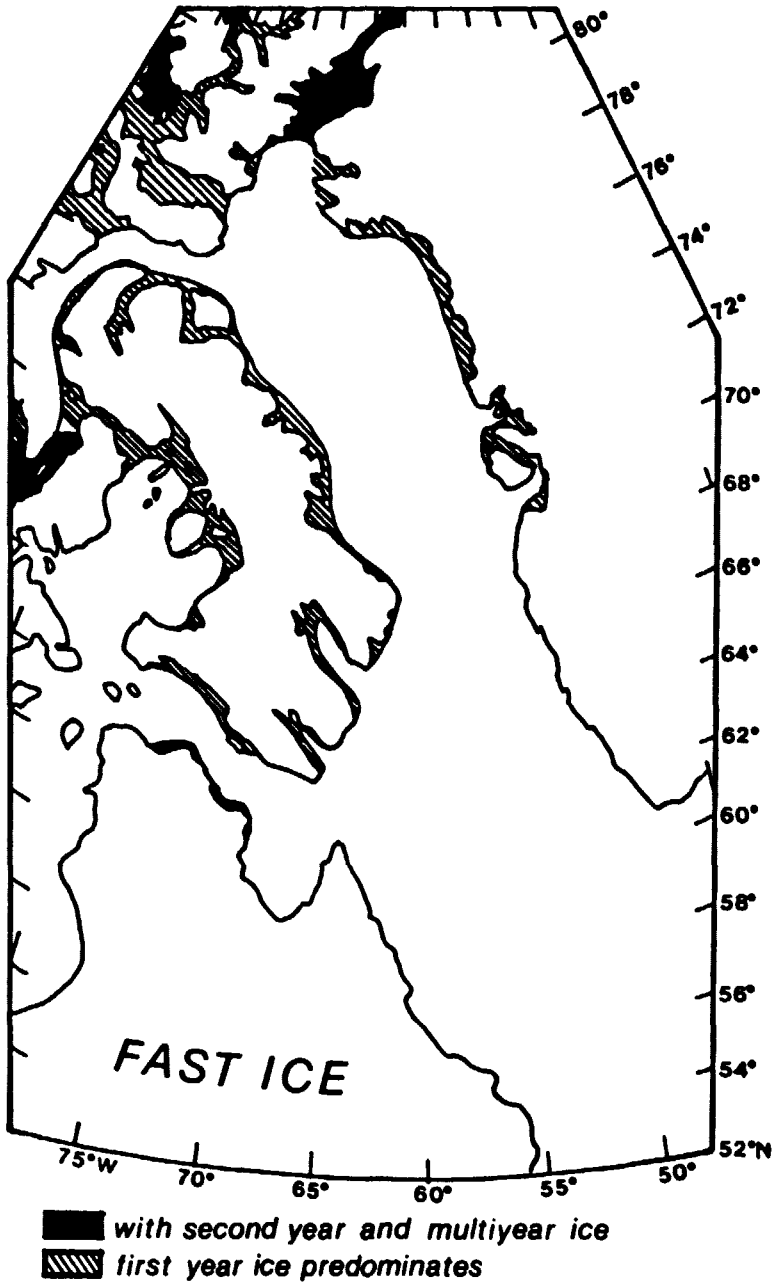

Figure 9

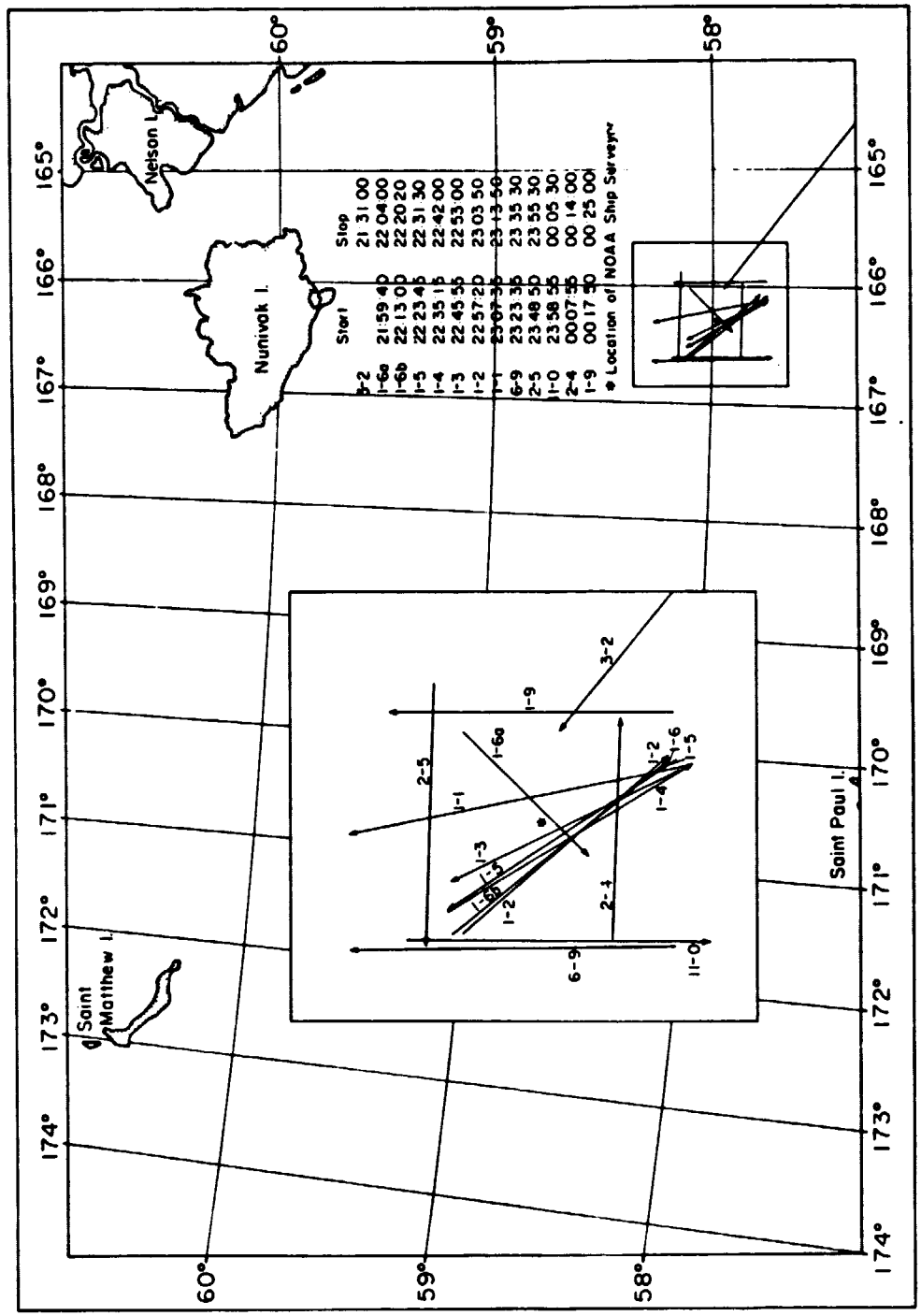

Figure 10

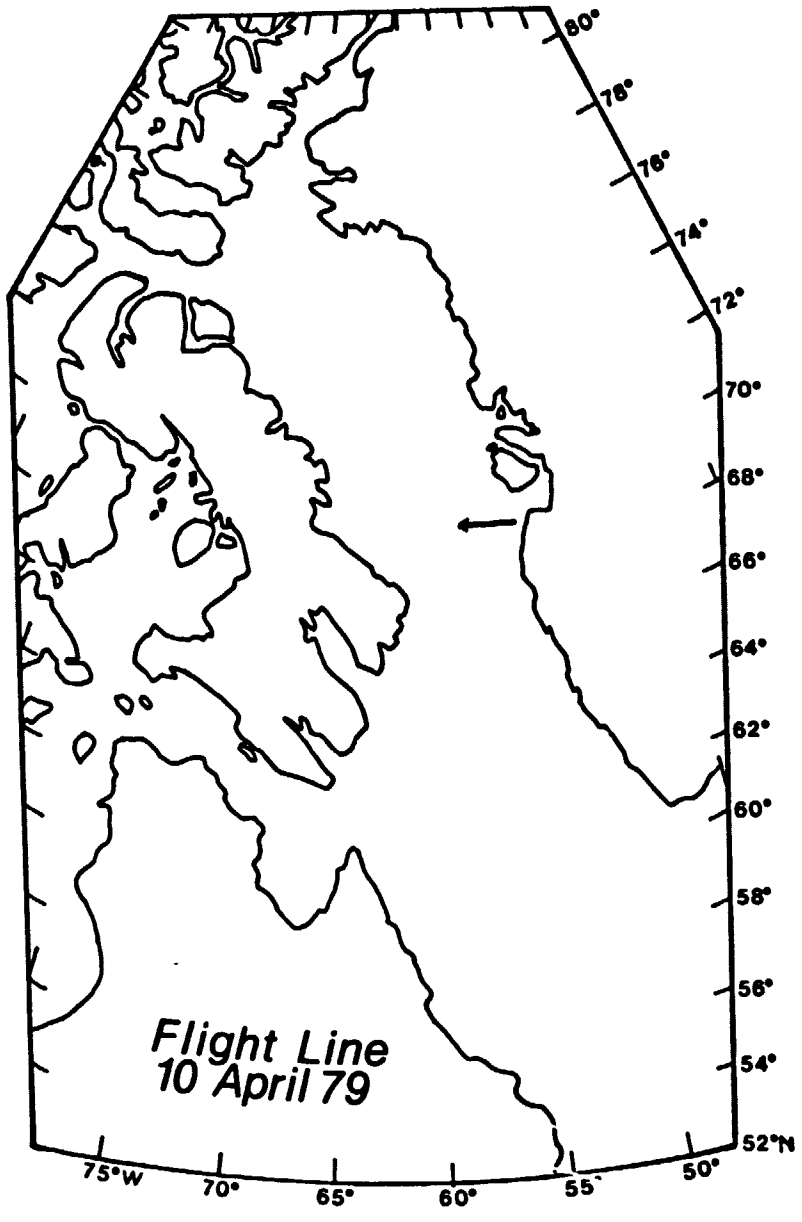

Figure 11

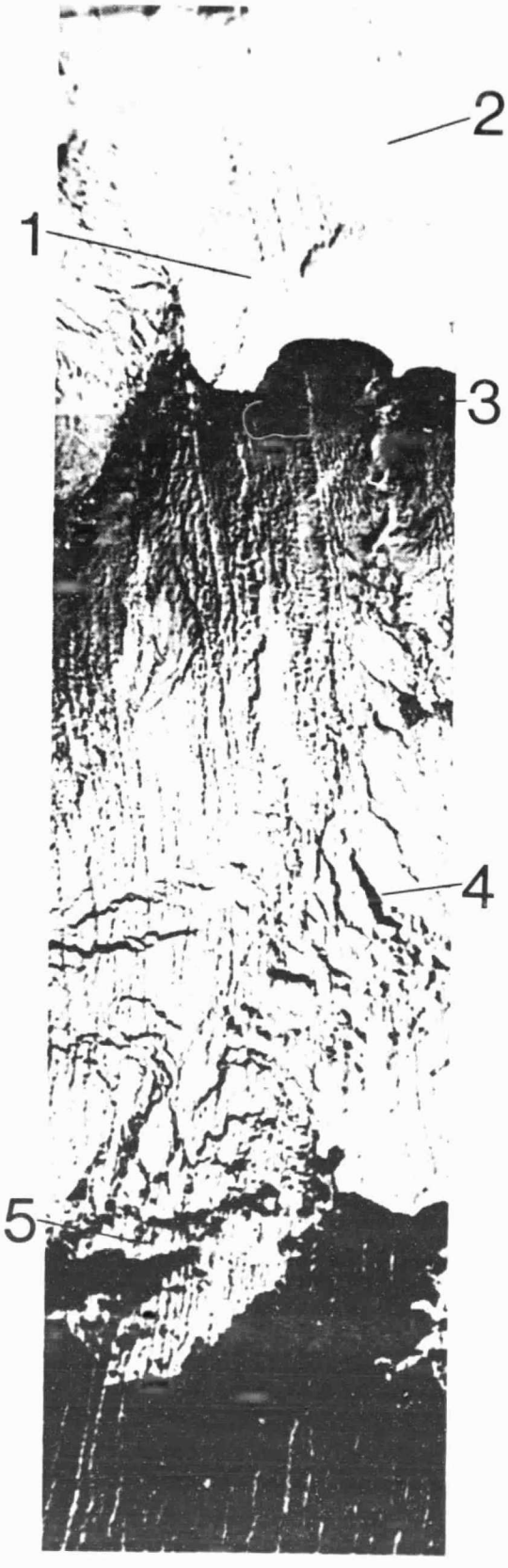

Figure 12

Figure 13

Figure 14

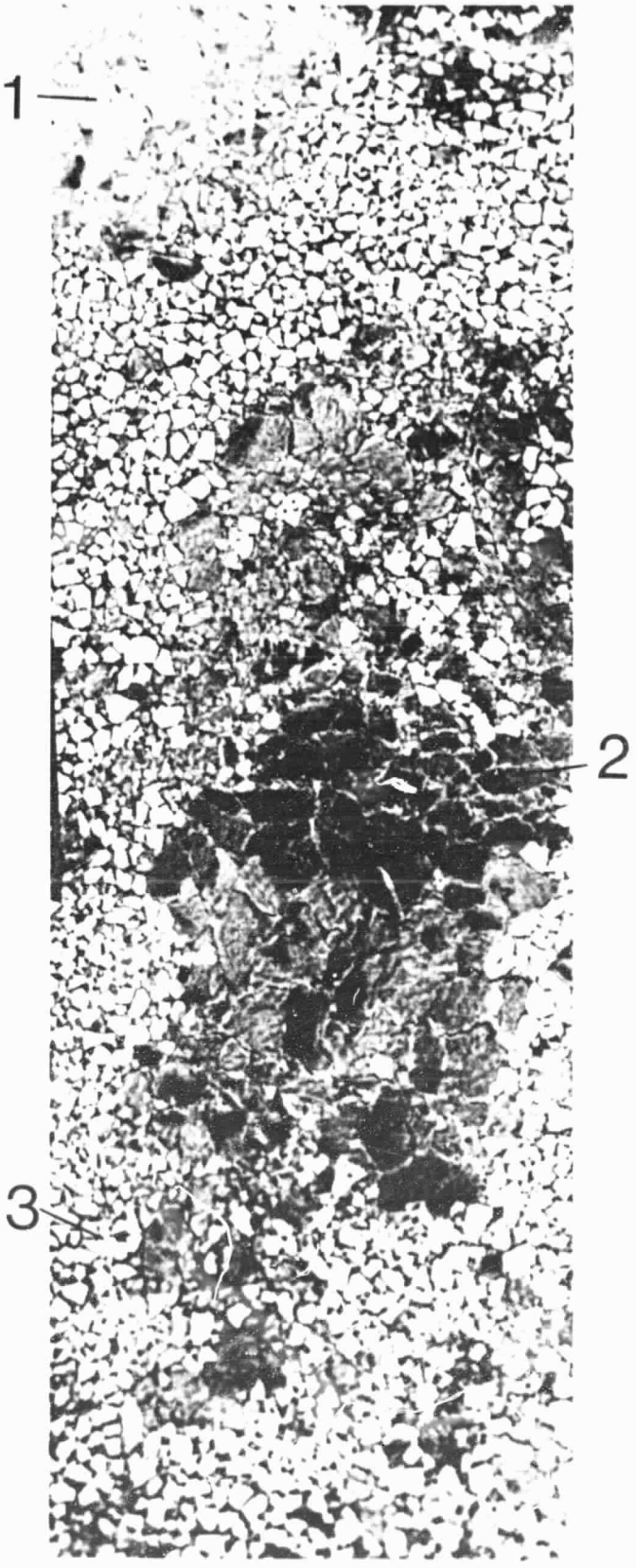

Figure 15

Figure 16

Figure 17

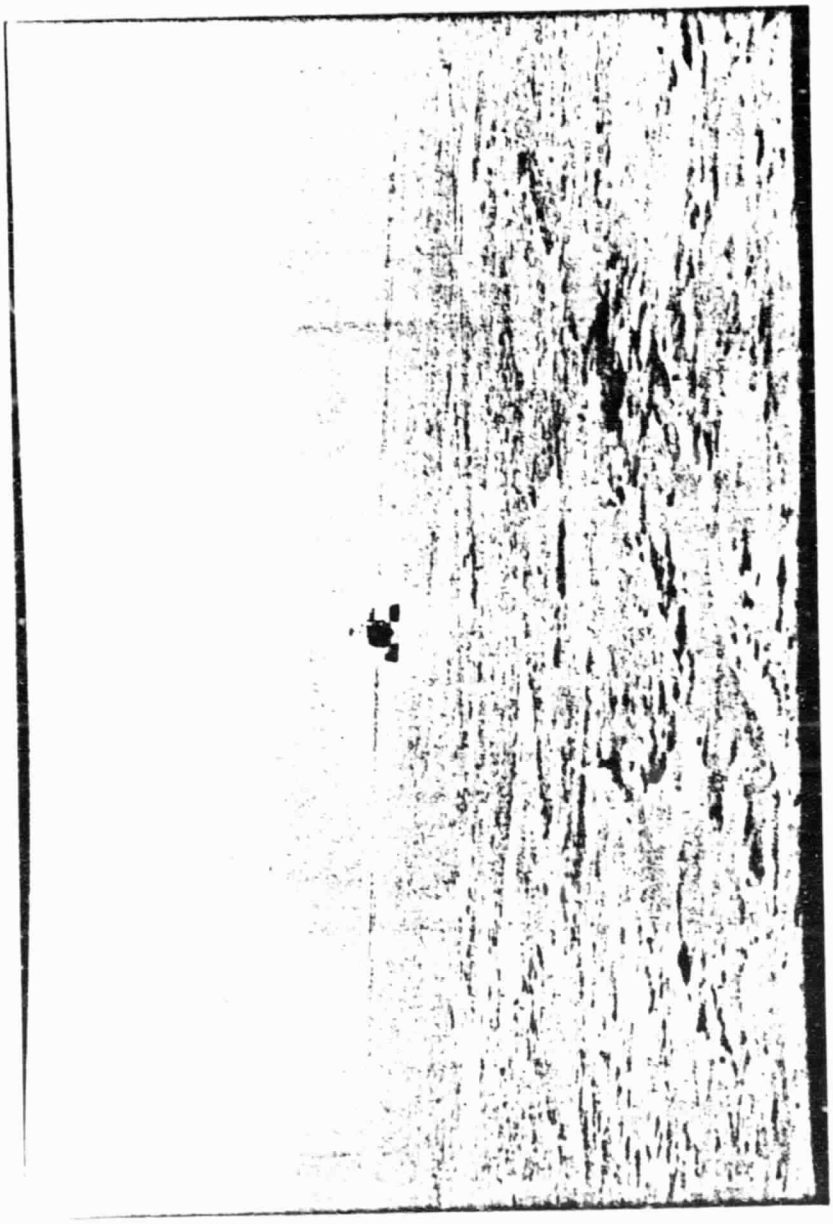

Figure 18

Figure 19

Figure 7

Figure 21

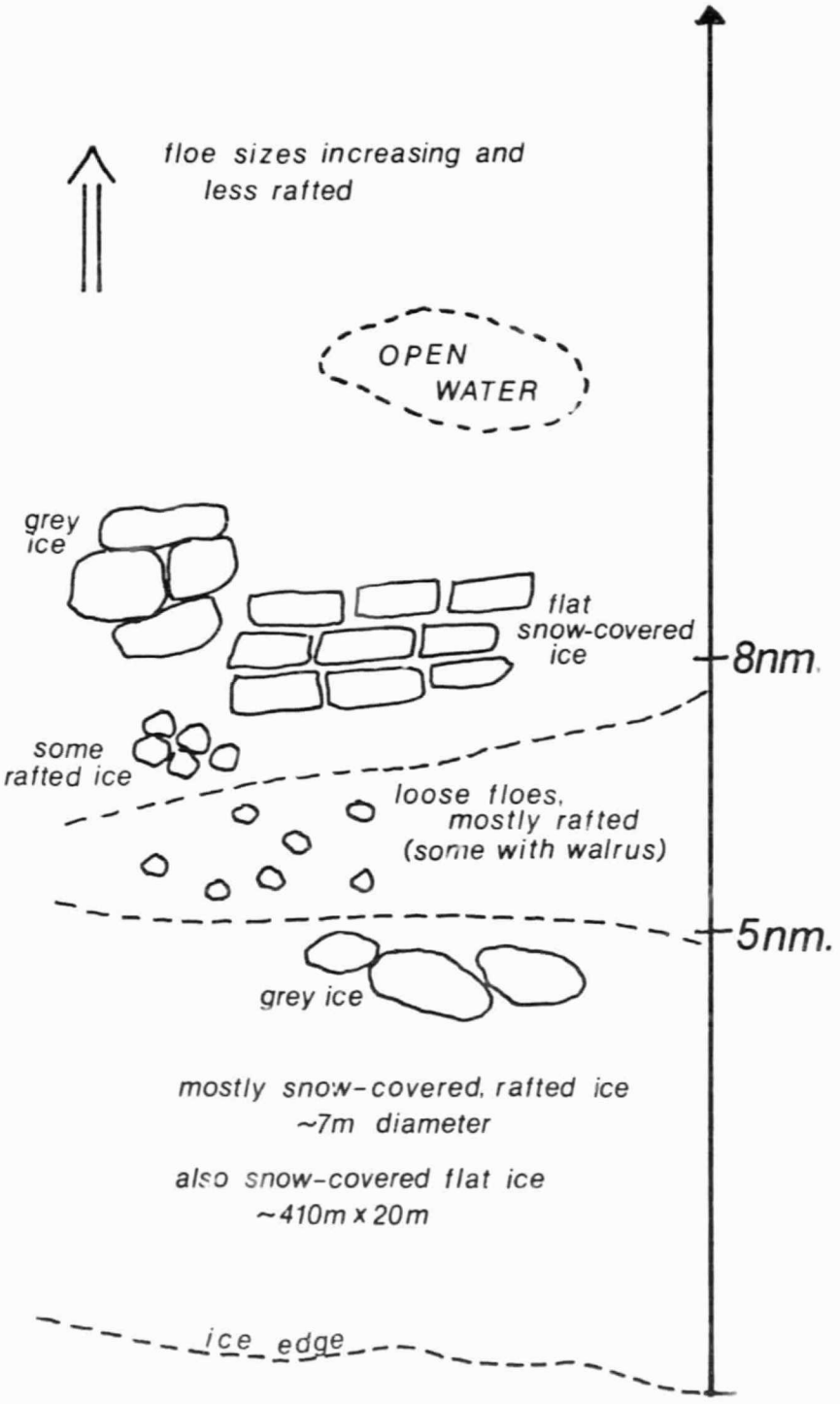

Figure 22

Figure 43

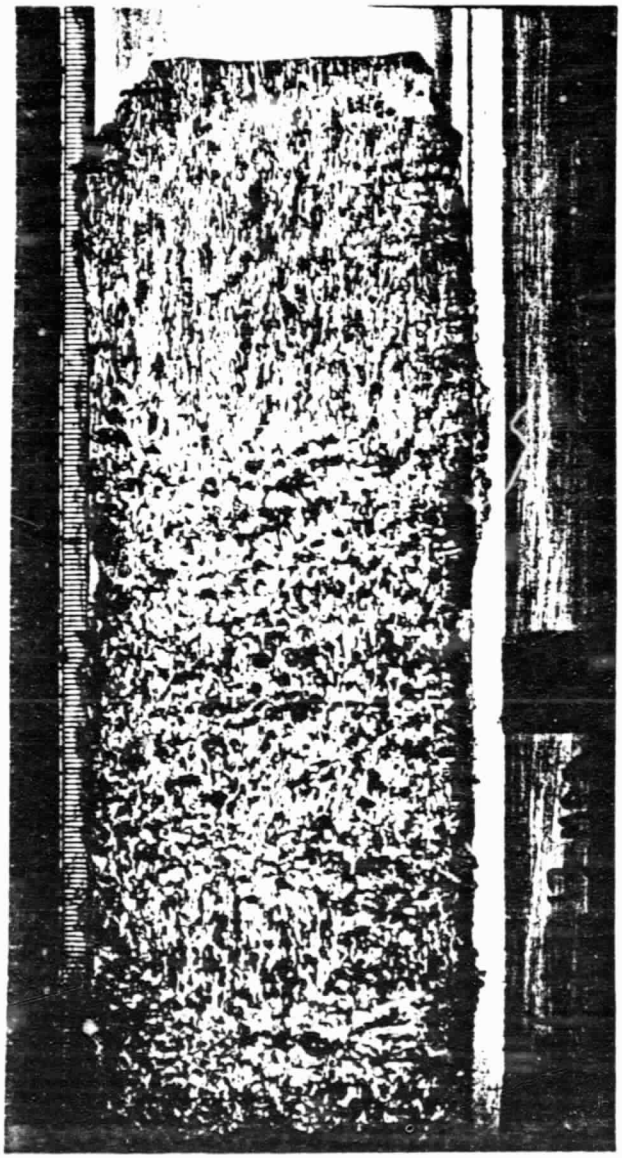

Figure 24

Figure 25

Figure 26

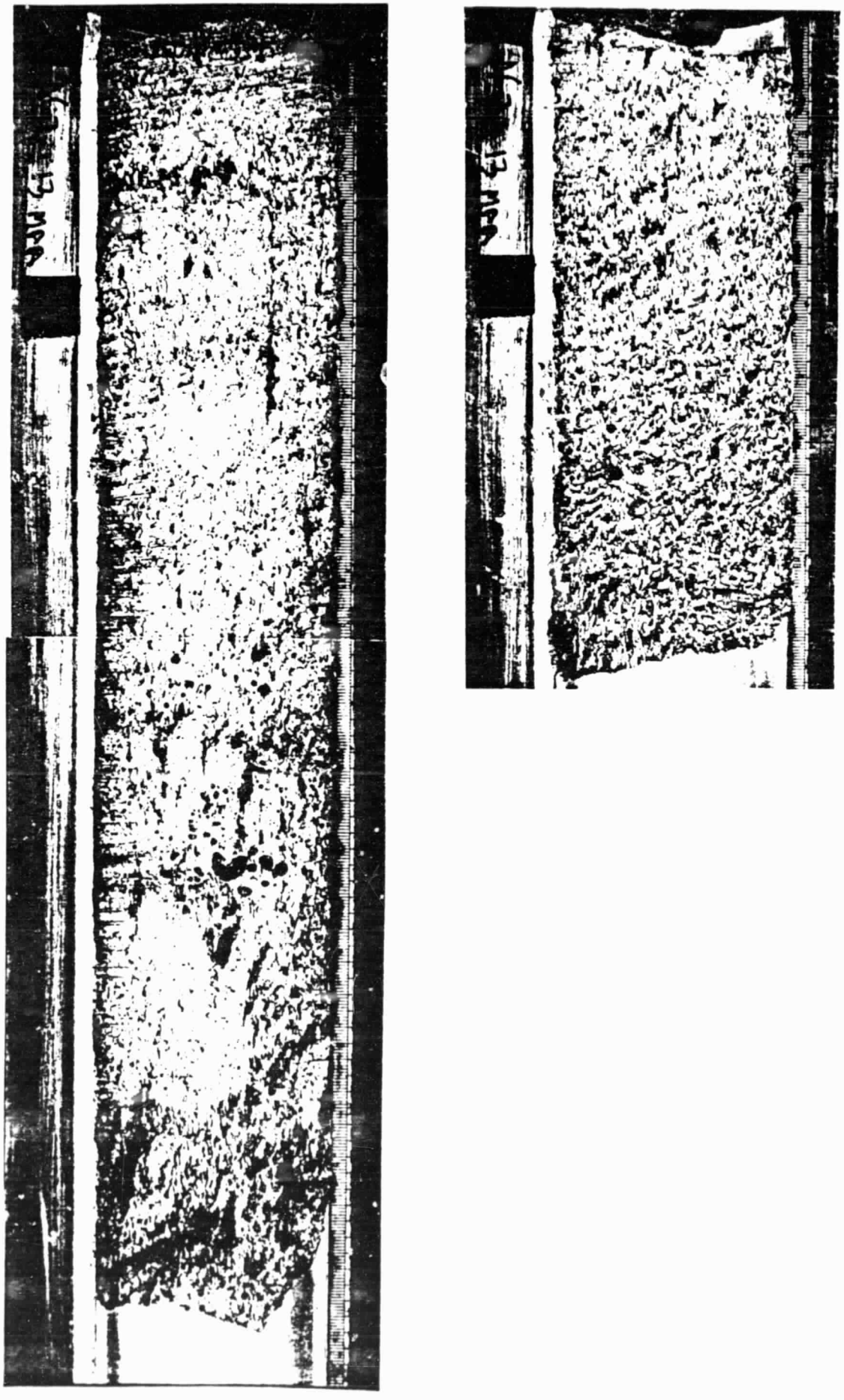

Figure 27

Figure 28

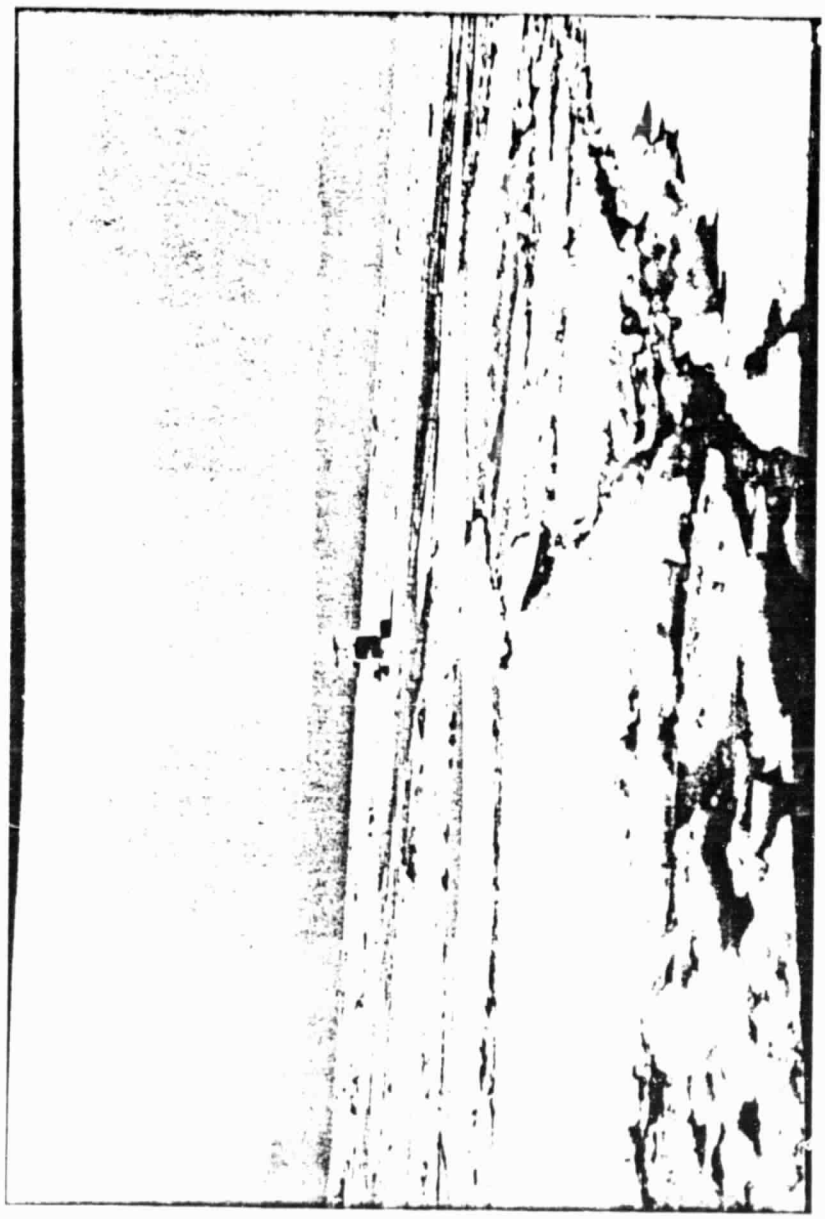

Figure 29

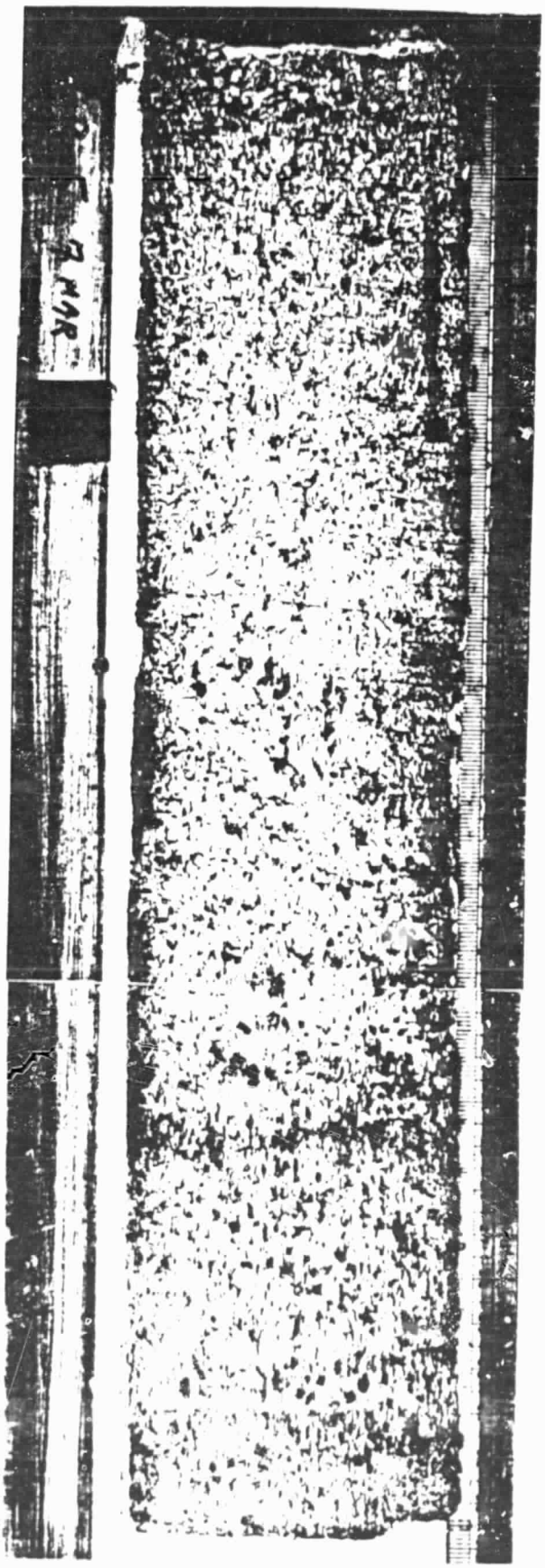

Figure 30

Figure 31

Figure 32

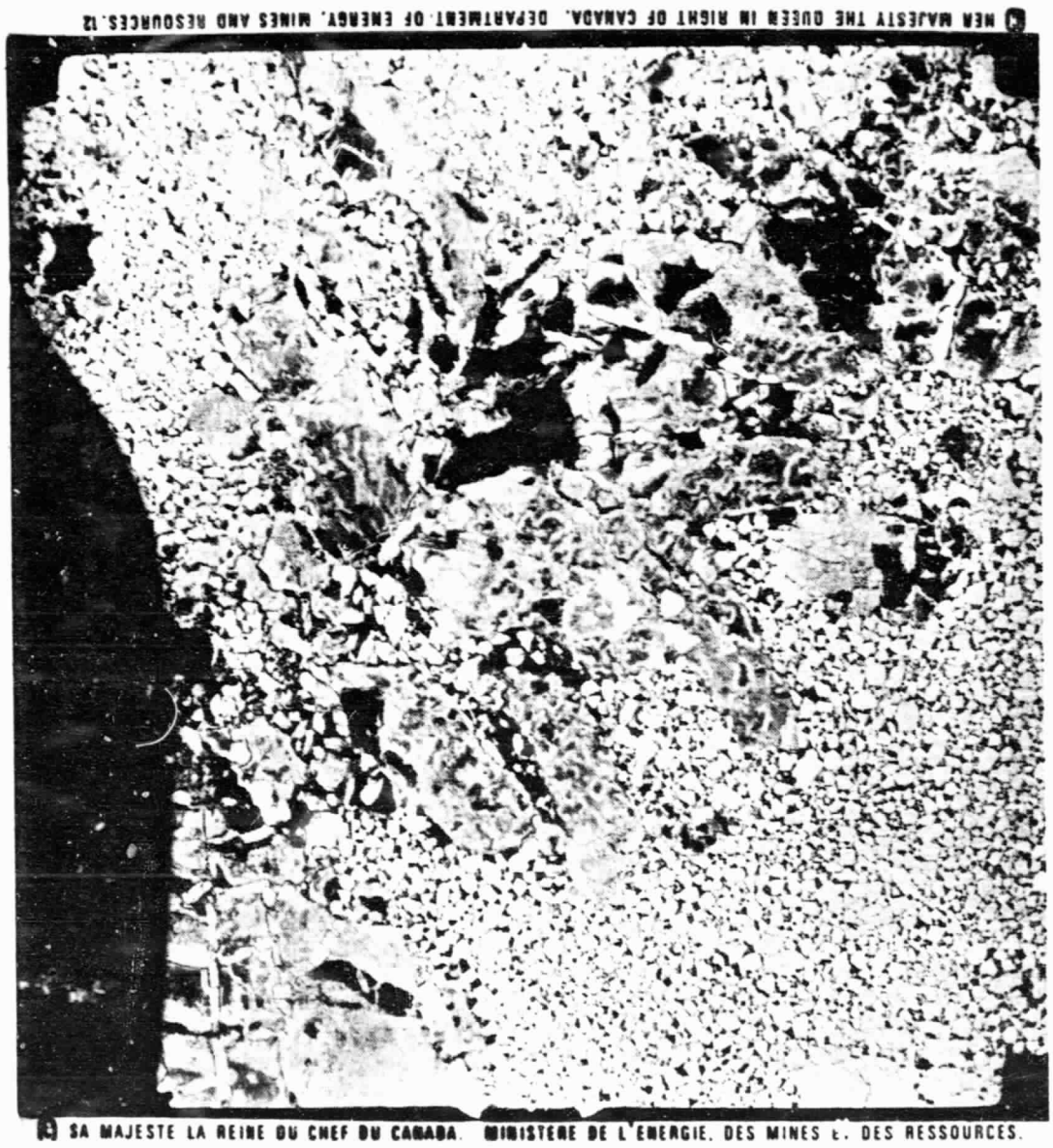

Figure 33

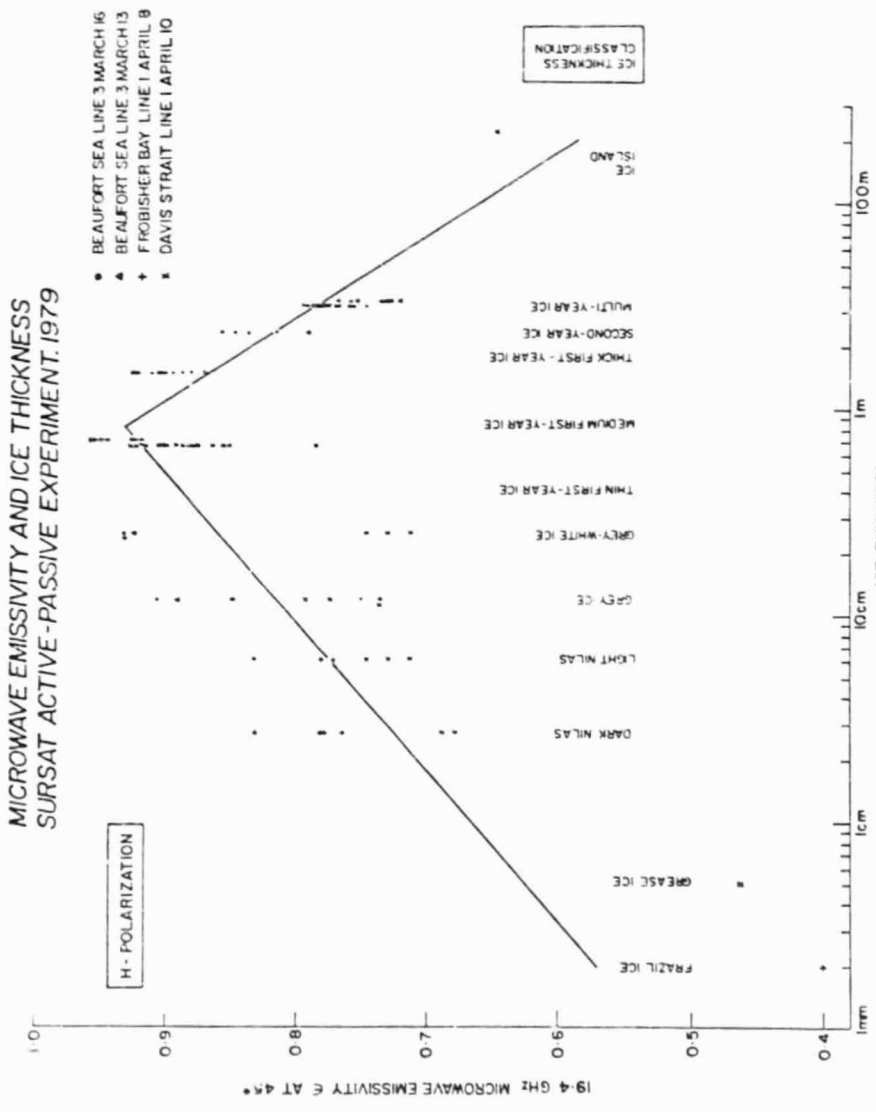

Figure 34

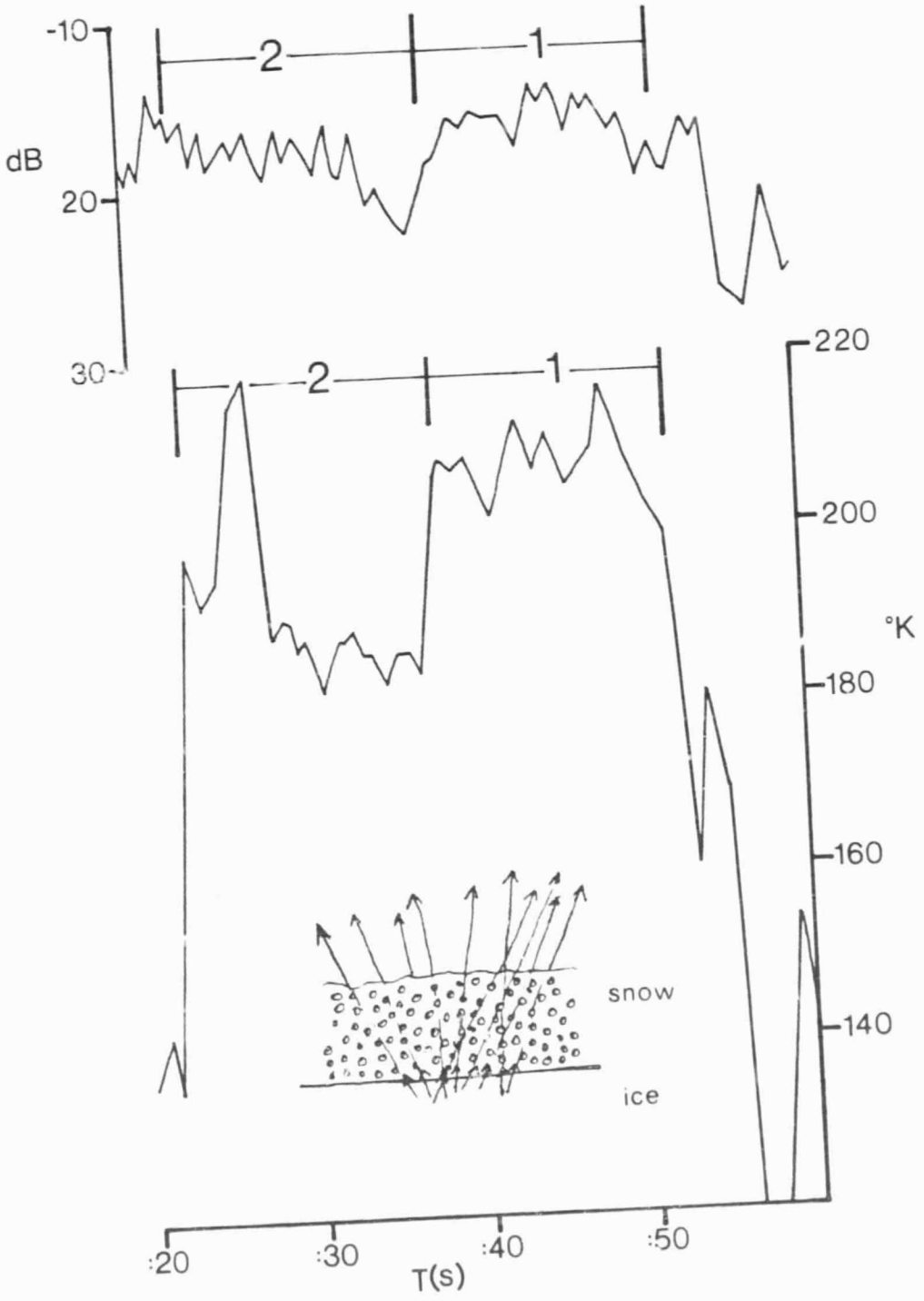

Figure 35

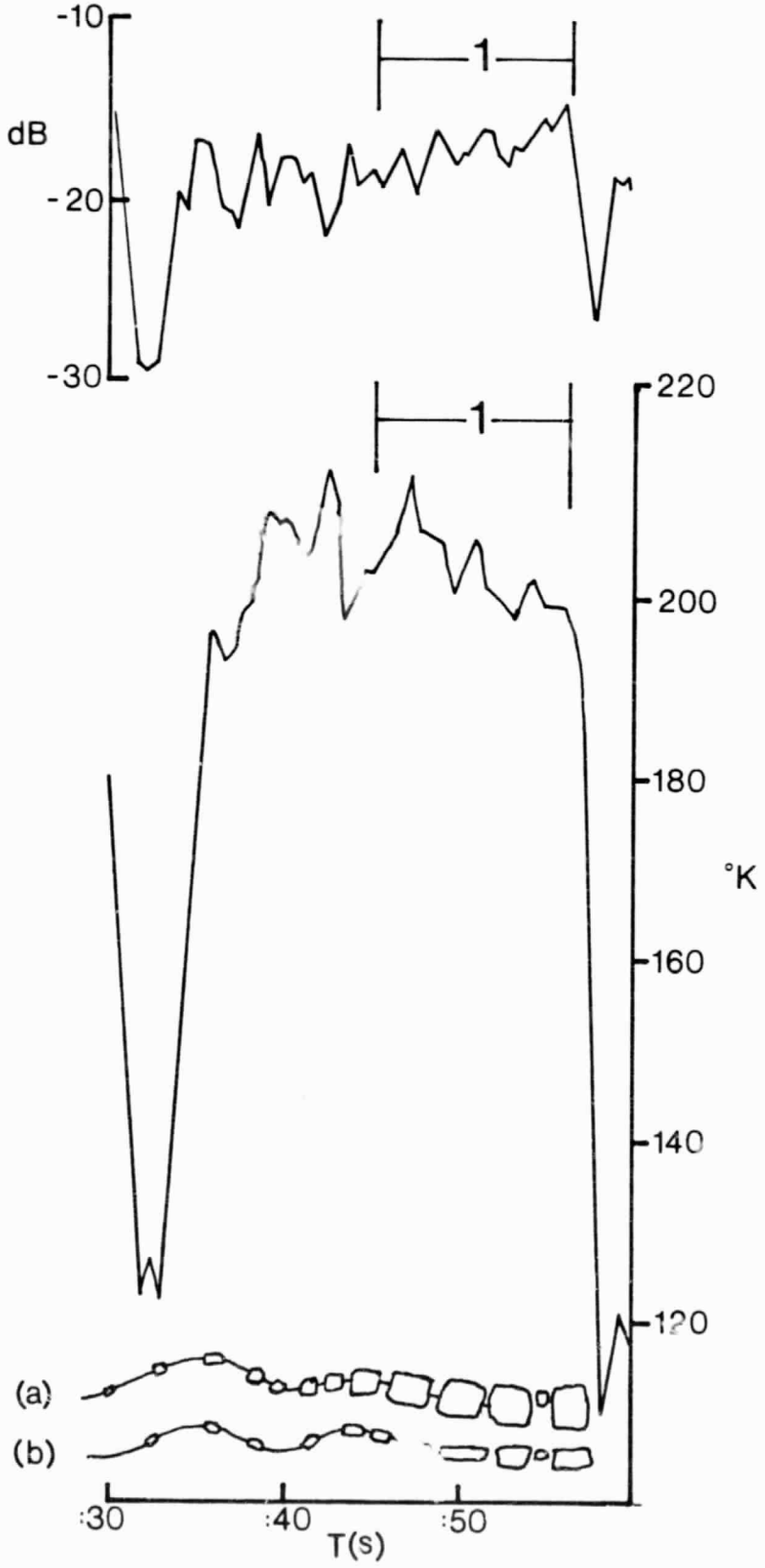

Figure 36

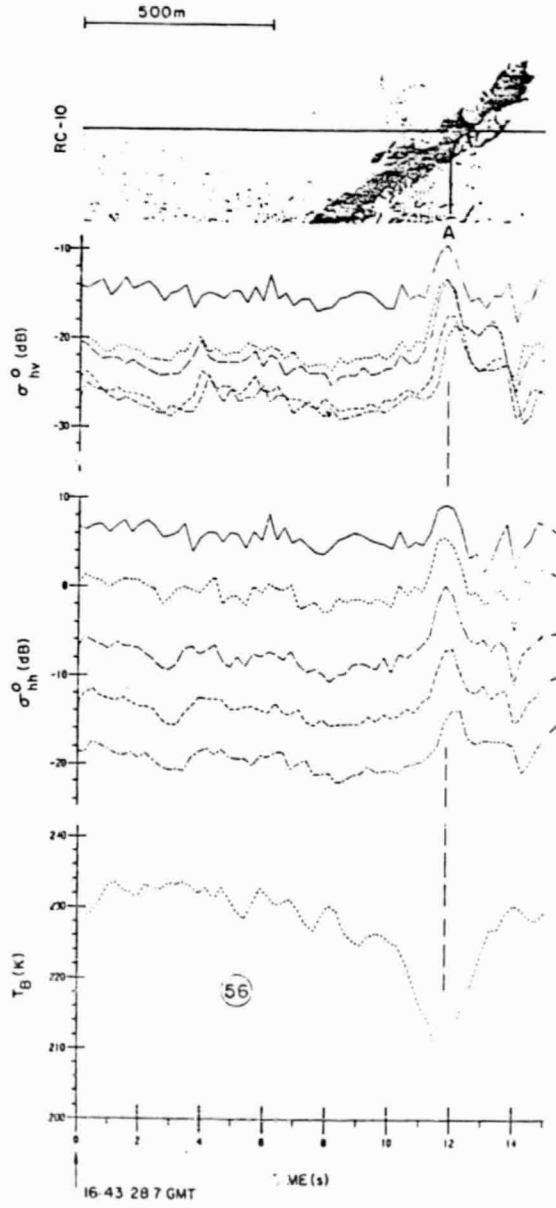

Figure A7.17.

ROTTEN, WET FIRST-YEAR ICE
DAVIS STRAIT
10 APRIL 1979
GRS-C FLIGHT LINE 1

13 3GHz BACKSCATTER COEFFICIENT

19 4 GHz BRIGHTNESS TEMPERATURE

Figure 37

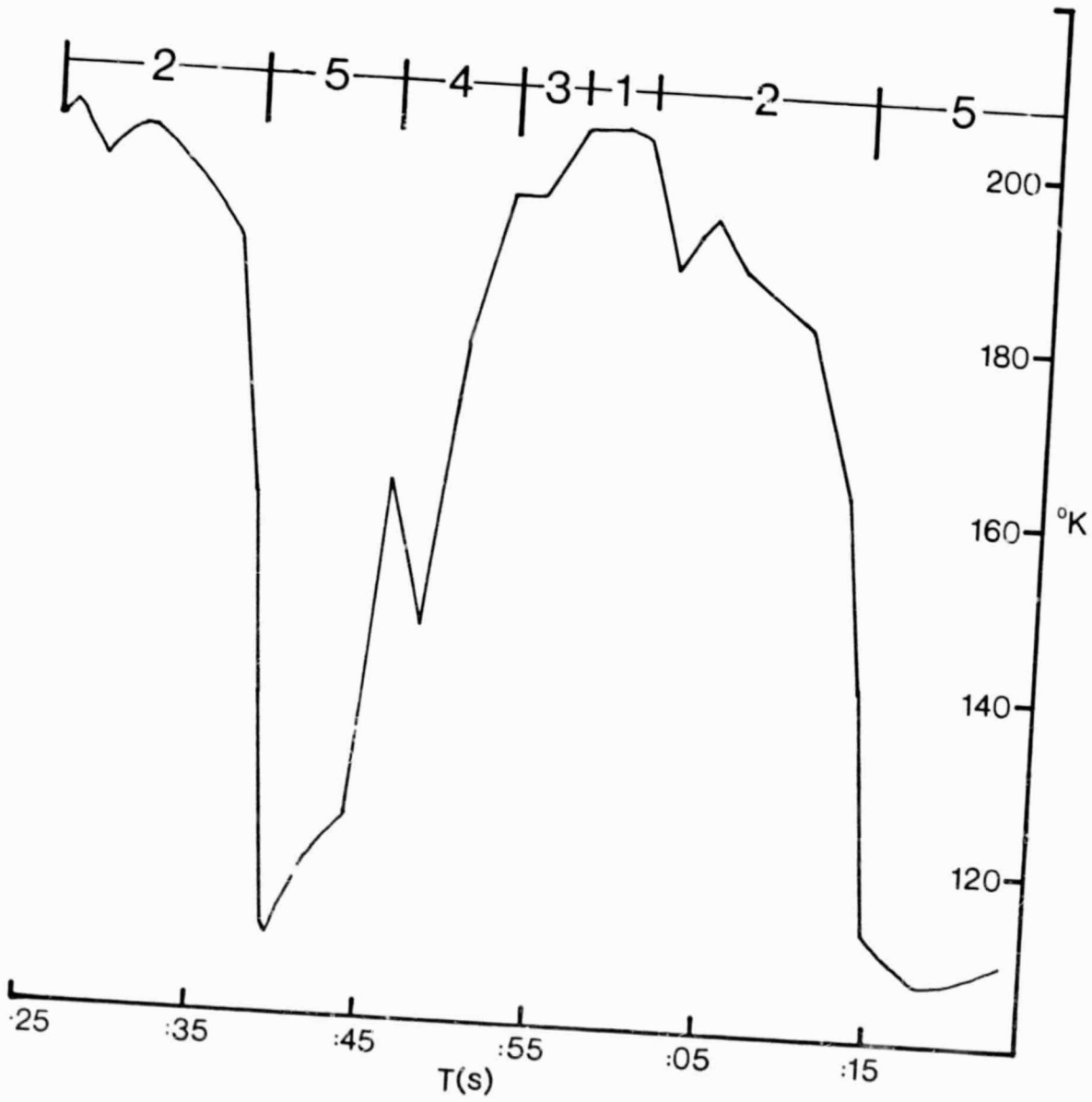

Figure 38

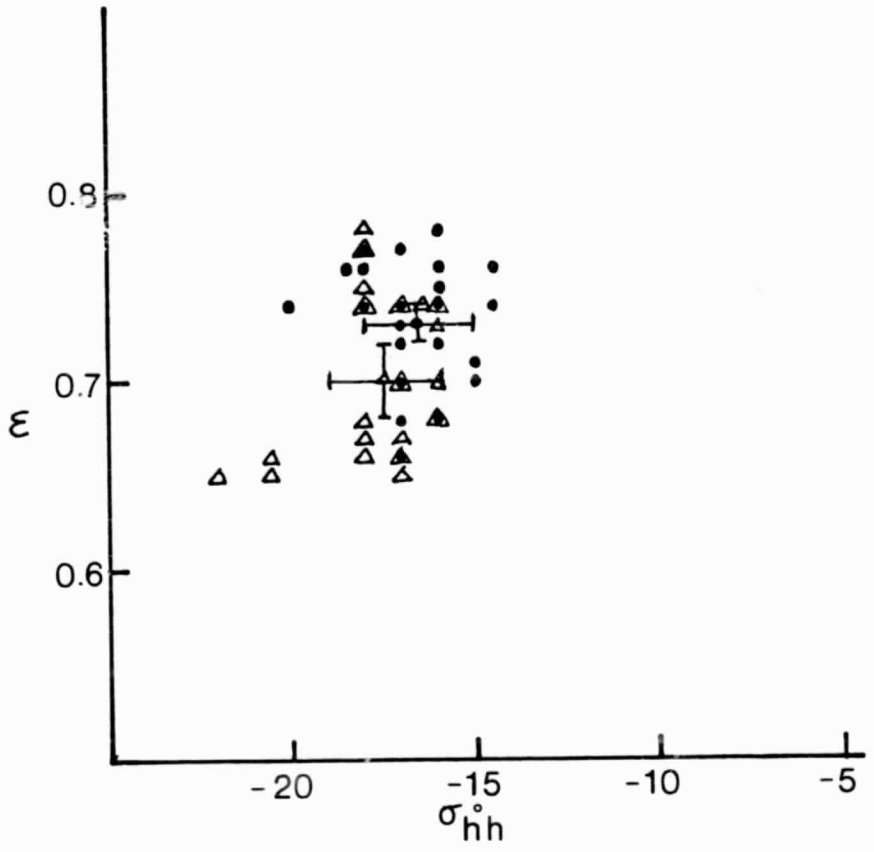

Figure 39

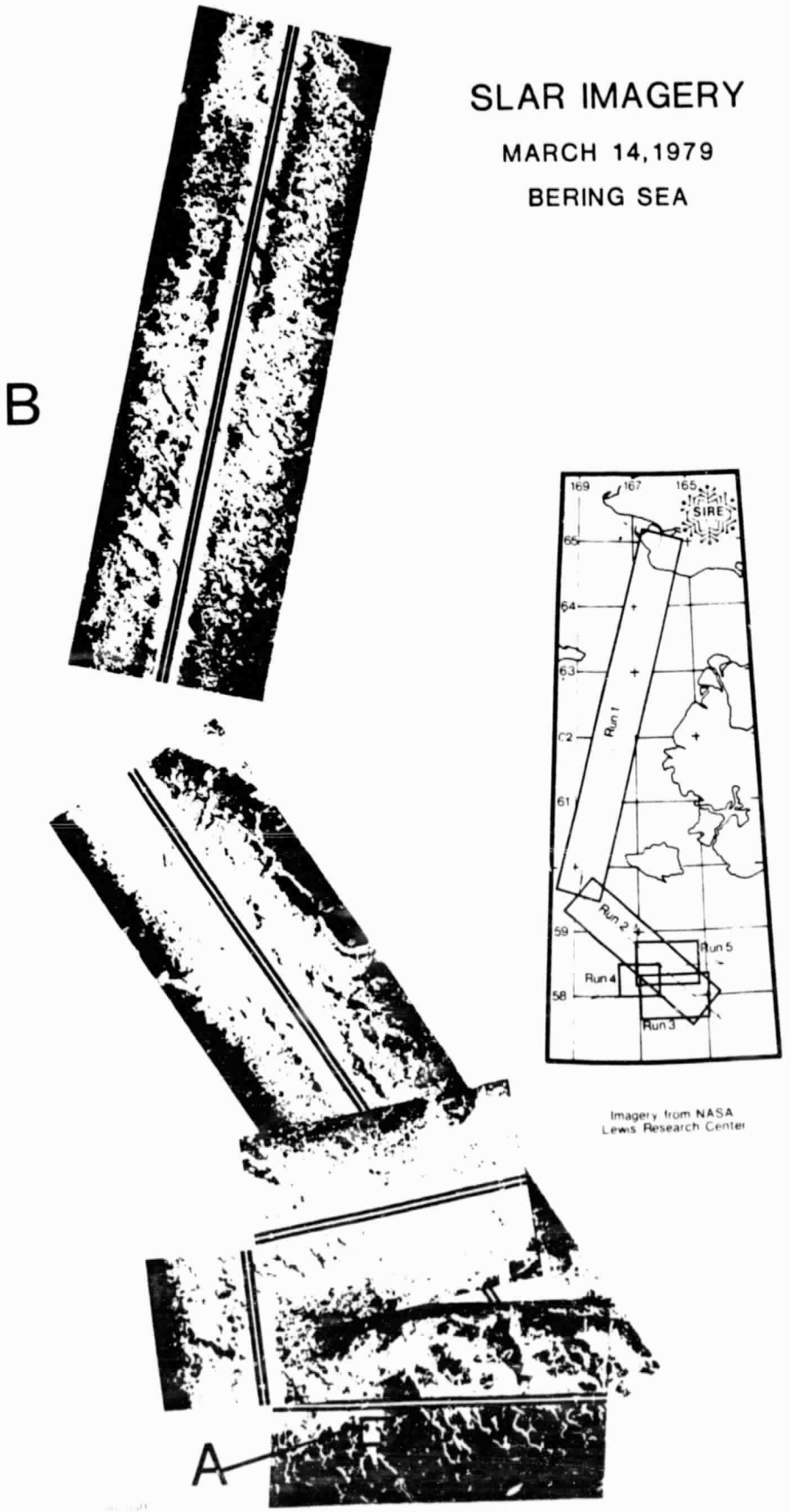

Figure 40

Figure 41

Figure 42

SLAR IMAGERY

MARCH 27, 1979

NORTON SOUND

Imagery from NASA Lewis Research Center

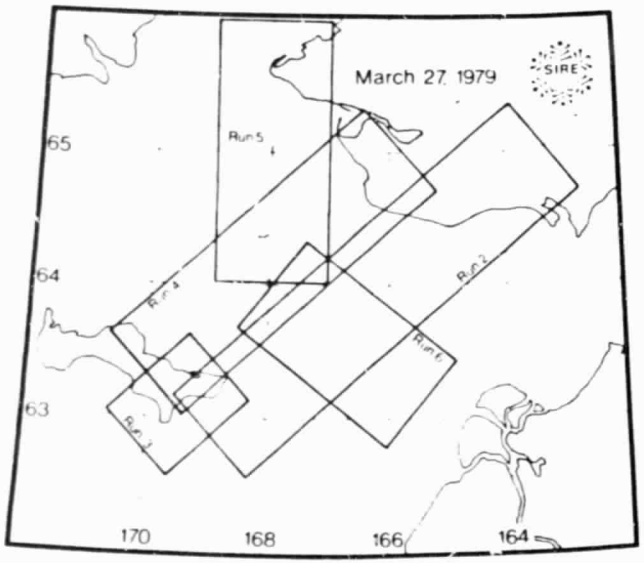

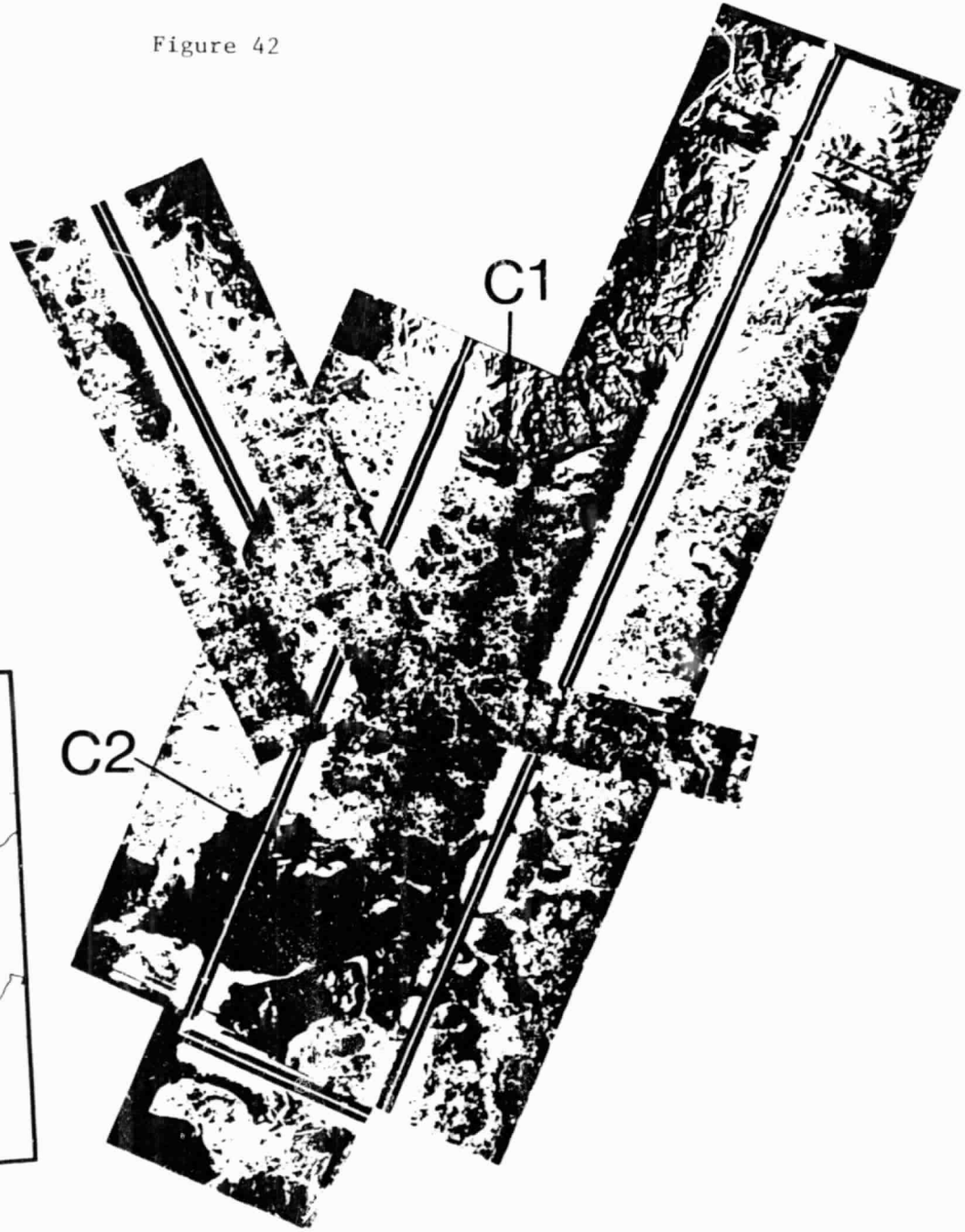

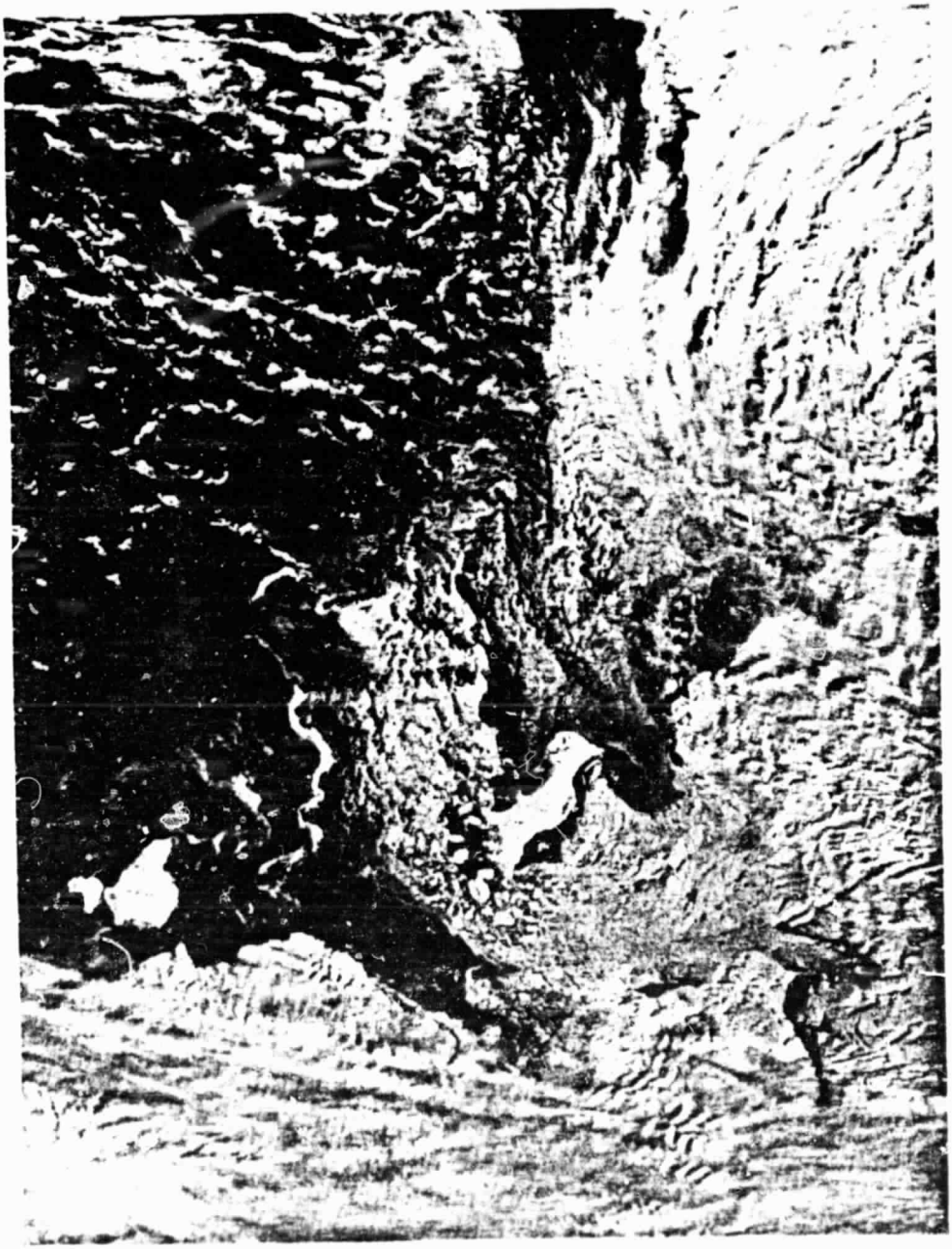

Figure 43